Available online at www.sciencedirect.com
SCIENCE DIRECT®
Pergamon
Progress in Oceanography 56 (2003) 281–321
Progress in Oceanography
www.elsevier.com/locate/pocean

The Portugal coastal counter current off NW Spain: new insights on its biogeochemical variability

X.A. Álvarez-Salgado [a,*], F.G. Figueiras [a], F.F. Pérez [a], S. Groom [b], E. Nogueira [a,c], A.V. Borges [d], L. Chou [e], C.G. Castro [a], G. Moncoiffé [f,g], A.F. Ríos [a], A.E.J. Miller [h], M. Frankignoulle [d], G. Savidge [f], R. Wollast [e]

[a] *CSIC, Instituto de Investigacións Mariñas, Eduardo Cabello 6, 36208 Vigo, Spain*
[b] *Plymouth Marine Laboratory, Prospect Place, Plymouth PL1 3DH, UK*
[c] *IEO, Centro Oceanográfico de Gijón, Avda. Príncipe de Asturias 70 bis, 33212 Gijon, Spain*
[d] *Unité d'Océanographie Chimique, Mare, University of Liège, Sart Tilman B5, B-4000 Liege, Belgium*
[e] *Laboratoire d'Océanographie Chimique et Géochimie des Eaux, Université Libre de Bruxelles, Campus de la Plaine—CP 208, B-1050 Brussels, Belgium*
[f] *Queen's University of Belfast, School of Biology and Biochemistry, Marine Laboratory, Portaferry, Co. Down, BT22 1PF, UK*
[g] *BODC, Bidston Observatory, Bidston Hill, Prenton CH43 7RA, UK*
[h] *SAMS, Dunstaffnage Marine Laboratory, University of the Highlands and Islands project, Oban, Argyll PA34 4AD, UK*

Abstract

Time series of wind-stress data, AVHRR and SeaWiFS satellite images, and in situ data from seven cruises are used to assemble a coherent picture of the hydrographic variability of the seas off the Northwest Iberian Peninsula from the onset (September–October) to the cessation (February–May) of the Portugal coastal counter current (PCCC). During this period the chemistry and the biology of the shelf, slope and ocean waters between 40° and 43°N have previously been undersampled. Novel information extracted from these observations relate to:

1. The most frequent modes of variability of the alongshore coastal winds, covering event, seasonal and long-term scales;
2. The conspicuous cycling between stratification and homogenisation observed in PCCC waters, which has key implications for the chemistry and biology of these waters;
3. The seasonal evolution of nitrite profiles in PCCC waters in relation to the stratification cycle;
4. The Redfield stoichiometry of the remineralisation of organic matter in Eastern North Atlantic Central Water (ENACW)—the water mass being transported by the PCCC;
5. The separation of coastal (mesotrophic) from PCCC (oligotrophic) planktonic populations by a downwelling front along the shelf, which oscillates to and fro across the shelf as a function of coastal wind intensity and continental runoff; and
6. The photosynthetic responses of the PCCC and coastal plankton populations to the changing stratification and light conditions from the onset to the cessation of the PCCC.

* Corresponding author. Tel.: +34-986-231-930; fax: +34-986-292-762.
E-mail address: xsalgado@iim.csic.es (X.A. Álvarez-Salgado).

0079-6611/03/$ - see front matter
doi:10.1016/S0079-6611(03)00007-7

Contents

1. Introduction

A poleward flowing slope undercurrent centred at depths of 150–300 m, which is compensating for the equatorward flows in the surface circulation, is a feature common to the coastal upwelling systems off California/Oregon, Peru/Chile, Namibia/Benguela and Canary/Iberian Peninsula (Smith, 1989). There is evidence for the existence of poleward undercurrents from tropical to polar latitudes along the eastern boundaries of all the major oceans (Pingree, 1994), which are primarily being forced by large-scale geopotential gradients and topography (Frouin, Fiúza, Ambar, & Boyd, 1990; Huthnance, 1995; McCreary, Shetye, & Kundu, 1986). Surface countercurrents also commonly feature in major coastal upwelling systems, either as the surface manifestations of trapped waves or as a result of undercurrents surfacing (Mooers, 1989). Such surfacing by undercurrents occurs in those latitudes that are affected by marked seasonal reversals in wind-stress and curl. Examples of such surfacing occur in the Hiada Current off Western

Nomenclature

α^B photosynthetic efficiency of P–E relationships (gC(gChl)$^{-1}$ h^{-1}) (µmol m^{-2} s^{-1})$^{-1}$
AOU apparent oxygen utilisation (µmol kg^{-1})
AVHRR advanced very high resolution radiometer
C_T total inorganic carbon (µmol kg^{-1})
CTZ coastal transition zone
DCM deep chlorophyll maximum
E_k light saturation parameter of P–E relationships (µmol m^{-2} s^{-1})
ENACW Eastern North Atlantic Central Water
ENACWsp ENACW of subpolar origin
ENACWst ENACW of subtropical origin
NAO 'North Atlantic Oscillation' index
NC_T C_T normalised to salinity 35.0 (µmol kg^{-1})
NTA TA normalised to salinity 35.0 (µmol kg^{-1})
PAR photosynthesis available radiation
PNM primary nitrite maximum
P^B_m maximum photosynthetic rate of P–E relationships (gC(gChl)$^{-1}$ h^{-1})
PCCC Portugal coastal counter current
P–E photosynthesis–irradiance relationships
PP primary production (mgC m^{-2} d^{-1})
$-Q_X$ offshore Ekman transport (m^3 s^{-1} km^{-1})
R continental runoff (m^3 s^{-1})
S[NAO] cumulative sum function of the NAO index
$S[-Q_X(t)]$ cumulative sum function of $-Q_X$
SC$[-Q_X]$ seasonal cycle of $-Q_X$
SeaWiFS sea-viewing Wide Field-of-view Sensor
SSS sea surface salinity
SST sea surface temperature (°C)
TA total alkalinity (µmol kg^{-1})

Canada (Freeland, 1989), the Davidson Current in the California Current System (Huyer, Kosro, Lentz, & Beardsley, 1989), and the Portugal coastal counter current (PCCC) off Portugal (Ambar & Fiúza, 1994). All these surface countercurrents manifest during autumn and winter, when local winds blow from the S–SW, forcing poleward displacement of the surface wind-mixed layer so that a convergent front developed in the coastal waters. An extreme case of a surface countercurrent is found in the Leeuwin Current, off Western Australia (Cresswell & Golding, 1980; Smith, Huyer, Godfrey, & Church, 1991). The largest alongshore geopotential gradients ever observed anywhere in eastern boundary regions prevent the development of a steady equatorward flow, despite the favourable wind-stress conditions during the spring and summer (Church, Cresswell, & Godfrey, 1989; McCreary et al., 1986).

The dynamics (fronts, centres and filaments) and biogeochemistry (primary production, recycling and shelf-ocean exchange) of coastal upwelling systems have been the subject of research conducted recently off California (Brink & Cowles, 1991), NW Africa (Barton et al., 1998) and NW Iberia (Joint et al., 2001) carried out under the auspices of the 'Coastal Transition Zone' programmes. Much less attention has been paid to the surface countercurrents that develop during prolonged downwelling-favourable periods lasting up to 6 months each year at temperate latitudes (Huyer et al., 1989; Wooster, Bakun, & Mclain, 1976).

The surface countercurrent regime not only transports salt, heat, dissolved substances and plankton assemblages from subtropical to temperate/subpolar latitudes along the slope but also prevents, or even reverses, the off-shelf export of materials that is normally characteristic of coastal upwelling systems (Pingree, Sinha, & Griffiths, 1999).

Ambar and Fiúza (1994) have reviewed the surface circulation off the Western Iberian Peninsula. This is an area dominated by the Portugal Current System, which is composed of the slow, equatorward, Iberian basin-scale flow of the Portugal Current proper in the open ocean (Arhan, Colin de Verdière and Memery, 1994; Krauss and Käse, 1984; Richardson, 1983); and the fast, seasonally reversing, Iberian slope scale flow of the Portugal Coastal Current near the coast. During summer, the Portugal Coastal Current is 30–40 km wide and 50–100 m deep and flows southward in the vicinity of the shelf break, being driven by upwelling-favourable northerly winds. It then transports recently upwelled, cold and nutrient-rich Eastern North Atlantic Central Water of subpolar origin (>45°N; ENACWsp) in the north, and warmer and nutrient-poor ENACW of subtropical origin (<40°N, ENACWst) in the south (Fiúza, 1984; Ríos, Pérez, & Fraga, 1992; Pérez, Mouriño, Fraga, & Ríos, 1993). In September–October the surface circulation reverses becoming the well-defined PCCC that is 30 km wide and 200 m deep flowing off the NW Iberian Peninsula, which is the subject of the present study. This mode of the PCCC persists until March–April (Ambar, Fiúza, Boyd, & Frouin, 1986; Frouin et al., 1990; Wooster et al., 1976), transporting ENACWst from at least 39°N (off Lisbon)—where it appears to be considerably wider—to the Armorican Shelf off SW France at 47°N (Pingree & Le Cann, 1990). Following Pingree, Sinha and Griffiths (1999), the coastal current system off NW Spain is considered to be a component of the predominantly density and topographically driven European 'Poleward Slope Current'.

The dynamics of the PCCC have been studied using AVHRR satellite images (Ambar et al., 1986; Pingree & Le Cann, 1990; Frouin et al., 1990), in situ hydrographic data accompanied by geostrophic calculations (Fiúza et al., 1998; Haynes & Barton, 1991; Mazé, Arhan, & Mercier, 1997), current meter records (Ambar et al., 1986; Swallow, Gould, & Saunders, 1977), and surface drifters (Haynes & Barton, 1990). However, little attention has been paid to the biogeochemical implications of the poleward surface flows either in the Portugal Current System or in the eastern boundary current systems in other oceans. Indeed, it appears that the studies by Bode, Fernández, Botas, and Anadón (1990) off N. Spain in April 1987 and Castro, Álvarez-Salgado, Figueiras, Pérez, and Fraga (1997) off NW Spain in September 1986 are unique in focusing on the biogeochemistry of these systems. Both studies found isolated communities of organisms associated with particular chemical (low NO_3^-, high NO_2^-) and physical conditions. More recently, Pelíz and Fiúza (1999) analysed coastal zone colour scanner (CZCS) images and found evidence for a wedge of southern oligotrophic water penetrating northward over the western Iberian continental margin during the autumn and winter, between the pigment-rich shelf zone and the zone of moderate concentrations further offshore.

Data from some of the seven research cruises involved in this study have previously been used to describe the thermohaline (Fiúza et al., 1998; Pérez, Ríos, King, & Pollard, 1995; Ríos, Pérez & Fraga, 1992) and chemical (Pérez, Castro, Álvarez-Salgado, & Ríos, 2001a,b; Pérez et al., 1993) characteristics of ENACW in the oceanic waters off NW Spain, the rapid ageing of ENACW on the shelf (Álvarez-Salgado, Castro, Pérez, & Fraga, 1997; Prego & Bao, 1997), the behaviour of surface waters as a source-sink for atmospheric CO_2 (Borges & Frankignoulle, 2002; Pérez, Ríos, & Rosón, 1998), and the estimates of primary production in NW Iberian shelf, slope and open ocean waters derived from satellite imagery (Joint et al., 2002). Consequently, this work will essentially focus on those aspects that have not yet been studied, namely:

1. A statistical approach to the recurrent modes of variability of coastal winds, covering from long-term to daily time-scales (Section 3.1);
2. The seasonal cycle of stratification and mixing of PCCC waters, which have key implications for the chemistry and biology of the area (Section 3.2.3);

3. The O_2/C/N/P/Si stochiometry of the mineralisation of organic matter in oceanic ENACW being transported by the PCCC (Section 3.3.1);
4. The seasonal evolution of nitrite profiles in PCCC waters in relation to the stratification conditions (Section 3.3.2);
5. The species composition of the phytoplankton communities in NW Iberian waters during the PCCC-favourable season (Section 3.4.2); and
6. The photosynthetic response of these species under contrasting conditions of the upper water column being either well-mixed or stratified (Section 3.4.3).

We will base our analyses on wind-stress and offshore Ekman transport calculations, AVHRR and SeaWiFS satellite images and a set of data from hydrographic cruises covering the onset of the PCCC (September–October), through the period of maximum winter convection to the cessation of the PCCC (April–May). The study will be restricted to latitudes between 40° and 43°N.

2. Materials and methods

2.1. The hydrographic cruises

Mapping of relevant thermohaline, chemical and biological variables was undertaken during seven hydrographic cruises conducted off the NW Iberian Peninsula between 1983 and 1998 (Fig. 1). Cruise GALICIA-XII (10–18 September 1991) coincided with the onset of the PCCC in the period of maximum stratification when there was the transition from upwelling- to downwelling-favourable winds. Cruises GALICIA-VI (1–12 December 1983) and MORENA-II (15 November–2 December 1993) took place when the development of the PCCC was in an advanced state of development in late autumn. The first of these two cruises was sampled between 42° and 44°N (off NW Spain), whereas the other extended the sampling further south from 42° to 40°N off Northern Portugal. Cruises CD110b (6–16 January 1998) and GALICIA-VII (18 February–7 March 1983) were carried out during the winter mixing period, and finally, cruise MORENA-I (10–26 May 1993) was conducted just before the onset of the upwelling season. Data from cruise Bg9815c (26 June–7 July 1998) will also be referred to in order to illustrate the situation when upwelling-favourable winds are predominant so that at the surface the Portugal Coastal Current flows southwards and the poleward flow is a subsurface slope undercurrent.

Cruises GALICIA-VI (December 1983) and GALICIA-VII (February–March 1984) were performed during the same downwelling season (1983–1984), which allows comparison of the hydrographic changes occurring in the PCCC before and after a winter mixing period in the same year, i.e. without any influence of interannual variability. Notable poleward surface flow occurred during the winter 1983–1984 resulting in conspicuous warming along the north Spanish coast around the New Year (Pingree & Le Cann, 1989). Similarly, cruises MORENA-I (May 1993) and MORENA-II (November–December 1993) were conducted before and after the upwelling-favourable season in 1993, thus allowing comparison of the spring and autumn PCCC within the same year. Although only four stations were occupied during CD110b (January 1998) because of bad weather, data from this cruise have been included because they provide a unique view of conditions during January.

Table 1 summarises the basic information about the cruises. Fig. 1 shows the locations of sampling sites where vertical profiles of the different variables were measured during each of the cruises. No plankton counts were carried out during the 1983–1984 cruises and primary production data are only available for cruises MORENA-I, GALICIA-XII, CD110b and Bg9815c.

Nutrient concentrations were determined by the 'Instituto de Investigacións Mariñas-Group of Oceanography' using standard segmented flow analysis techniques (Álvarez-Salgado, Fraga, & Pérez, 1992;

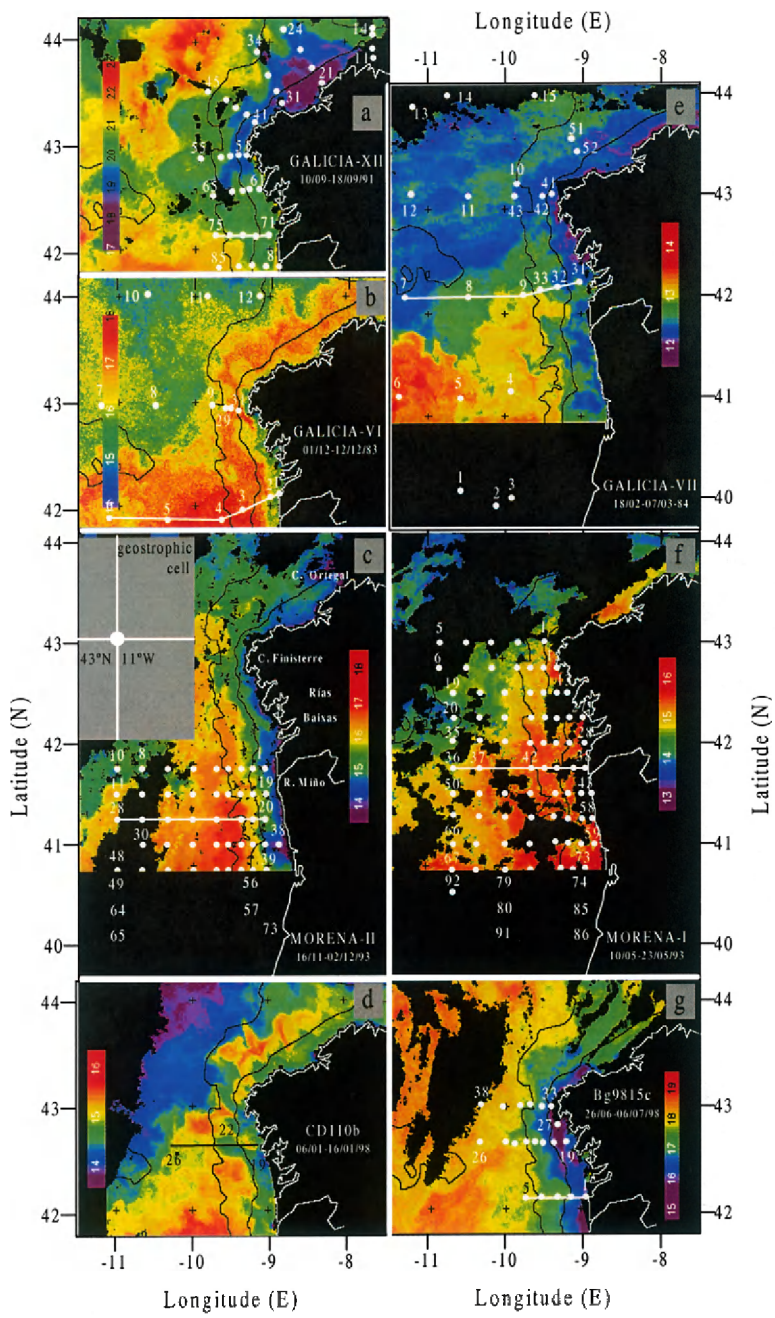

Fig. 1. Map of the survey area (NW Iberian Peninsula) for the set of seven cruises included in this work: GALICIA-XII (September 1991) (a), GALICIA-VI (November–December 1983) (b), MORENA-II (November 1993) (c), CD110b (January 1998) (d), GALICIA-VII (February–March 1984) (e), MORENA-I (May 1993) (f), and Bg9815c (July 1998) (g). White points show the position of the stations occupied on each cruise. Solid lines represent the cross-shelf sections used in Figs. 6, 7, 9, 10, 13 and 14. The 2° × 2° geostrophic-wind cell centred at 43°N 11°W (−11°E) is presented in chart c. The 200 and 1000 m isobaths are also included. AVHRR images correspond to the sampling dates and are the most representative for the SST distribution found during the cruises. Major geographic features are presented in panel c.

Table 1
Relevant information about the cruises referred to in this study, including sampling dates, vessel, gear, measured variables and prevailing oceanographic conditions

Cruise	Dates	Vessel	Sampling gear	Measured variables					Oceanographic scenario	
				θ/S	Nut	Chl	Plank	PP	Prevailing winds, m s^{-1}	PCCC conditions
GALICIA-VI	1–12 December 1983	C. de Saavedra	Niskin bott., inv. therm.	×	×	×			Southerly, 6.2	Late autumn PCCC-favour. cond.
GALICIA-VII	18 February–7 March 1984	C. de Saavedra	Niskin bott., inv. therm.	×	×	×			North easterly, 8.2	Late winter PCCC-favour. cond.
GALICIA-XII	10–18 September 1991	Investigador S.	CTD, rosette sampler	×	×	×	×	×	Westerly, 4.5	PCCC onset
MORENA-I	10–26 May 1993	C. de Saavedra	CTD, rosette sampler	×	×	×	×	×	South westerly, 6.3	PCCC cessation
MORENA-II	15 November–2 December 1993	Hakon Mosby	CTD, rosette sampler	×	×	×	×		Southerly, 7.0	Late autumn PCCC-favour. cond.
CD110b	6–16 January 1998	Charles Darwin	CTD, rosette sampler	×	×	×	×	×	Southerly, 15	Early winter PCCC-favour. cond.
BG9815Cc	26 June–7 July 1998	Belgica	CTD, rosette sampler	×	×	×	×	×	North easterly, 12	PCCC unfavour. (upwelling-favour.)

Hansen & Grasshoff, 1983; Mouriño & Fraga, 1985). Potentiometric pH was measured in the National Bureau of Standards (NBS) scale with the classical 7.413 phosphate buffer in most cruises, following the procedure of Pérez and Fraga (1987a). During cruises CD110b and Bg9815c the electrode was calibrated in the Total Hydrogen Ion Concentration Scale with the TRIS and AMP buffers according to Dickson (1993). Total alkalinity (TA) was measured by potentiometric end-point titration according to Pérez and Fraga (1987b), except on cruises CD110b and Bg9815c when classical Gran electro-titration was used. Total inorganic carbon (C_T) was calculated from pH and TA using the carbon system equations. C_T and TA have been normalised to salinity 35.0 to produce the corresponding NC_T and NTA parameters, which depend only on the biological and geochemical activity in the water sampled. Finally, dissolved oxygen was measured by the Winkler method using a potentiometric end-point determination. Apparent oxygen utilisation, $AOU = O_2sat - O_2$, has been calculated using Benson and Krause's equation (UNESCO, 1986)

for oxygen saturation (O_2sat). Chlorophyll *a* (Chl-*a*) was estimated fluorometrically by the method of Yentsch and Menzel (1963).

2.2. Wind-stress and offshore–onshore Ekman transport calculations

The north (south) component of shelf wind-stress (τ_y) causes upwelling (downwelling) favourable offshore (onshore) Ekman transport values ($-Q_X$) along the NW Iberian margin (Wooster et al., 1976), which can be roughly estimated following Bakun's (1973) method

$$-Q_x = \frac{\tau_y}{\rho_{SW}.f} = -\frac{\rho_{air}.C_D.|V|.V_y}{\rho_{SW}.f}, \quad (1)$$

where ρ_{air} is the density of air (1.22 kg·m^{-3} at 15 °C), C_D an empirical dimensionless drag coefficient (1.4×10^{-3} according to Hidy, 1972), f the Coriolis parameter (9.946×10^{-5} s^{-1} at 43° latitude), ρ_{SW} the density of seawater (~1025 kg m^{-3}) and $|V|$ and V_y are the average daily module and north component of the geostrophic winds in a 2° × 2° cell centred at 43°N 11°W (Fig. 1(c)) assumed representative for the study area. Average daily geostrophic winds were estimated from atmospheric surface pressure charts, provided at 6 h intervals by the 'Instituto Nacional de Meteorología'. Positive values of $-Q_X$ (m^3 s^{-1} km^{-1}) indicate upwelling-favourable offshore Ekman transport. Conversely, negative values of $-Q_X$ indicate downwelling-favourable onshore Ekman transport (see Lavín, Díaz del Río, Cabanas, & Casas, 1991, for further details).

The time series of daily values of $-Q_X$ from August 1981 to July 1998 ($n = 6205$) has been analysed (Fig. 2(a)). Values outside the lower extreme bound (LEB = $Q_1 - 3H = -3200$ m^3 s^{-1} km^{-1}) and upper extreme bound (UEB = $Q_3 + 3H = 3022$ m^3 s^{-1} km^{-1}) were rejected and the time series was analysed (Q_1 and Q_3 are the lower and upper quartiles and H is the interquartile range). The rejected values represented ~3% of the whole time series. Spectral and harmonic analyses (Poularikas & Seely, 1991), and differencing techniques (Ibanez, Dauvin, & Ettienne, 1993) were applied to characterise the modes of temporal variability of $-Q_X$ from short-term to interannual scales.

2.3. Geostrophic flow calculations

Following Frouin et al. (1990), the geopotential anomaly at 10 dbar was computed relative to 350 dbar. Although water displacements at this reference level are significant (Mazé et al., 1997), they are small compared to the enhanced surface circulation in the area during either the upwelling- or the downwelling-favourable seasons. Therefore, strictly, our geostrophic computations only provide a qualitative, rather than a quantitative, description of the geostrophic circulation patterns. A more appropriate reference level would have been 2500 dbar (Mazé et al., 1997), but on some of the cruises (GALICIA-XII, MORENA-II and Bg9815c) it was not possible to sample to this depth. Comparison of the geopotential anomalies at 10 dbar referred to 350 and 2500 dbar for the MORENA-I cruise showed a reasonable correlation ($r = +0.79$, $p < 0.05$). For shelf stations, where the water depth (Z) is shallower than the reference level, the extrapolation method of Reid and Mantyla (1976) was used, which consists of extrapolating the horizontal gradients of the geopotential anomaly computed from the pairs of stations in deeper waters towards the stations with $Z < 350$ dbar.

2.4. AVHRR and SeaWIFS images

2.4.1. Sea-surface temperature

Sea-surface temperature was measured using the advanced very high resolution radiometer (AVHRR) series of instruments, flown on the US NOAA series of polar-orbiting satellites. Individual 1-km resolution,

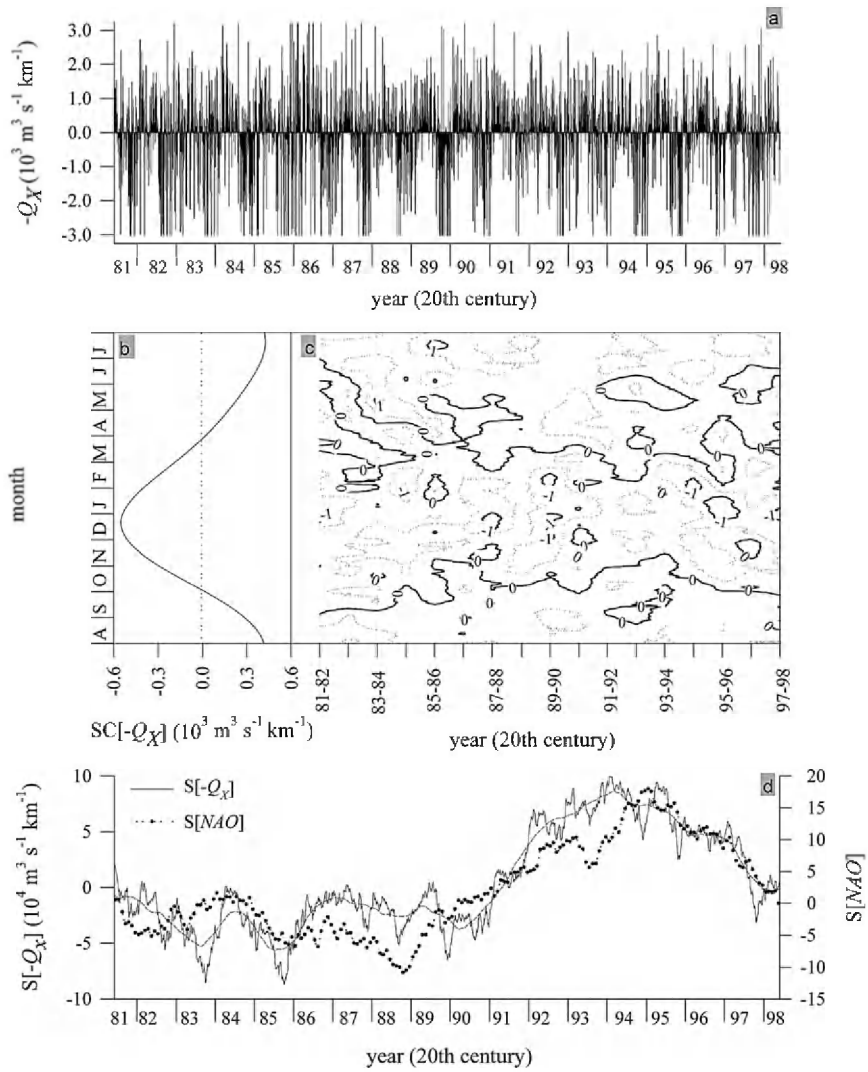

Fig. 2. Offshore Ekman transport values ($-Q_X$) calculated from the wind field at the 2° × 2° geostrophic cell centred at 43°N 11°W (−11°E) for the period August 1981–August 1998. (a) Time series of daily values of $-Q_X$ (in 10^3 m^3 s^{-1} km^{-1}). Positive (negative) values indicate upwelling (downwelling) favourable winds. (b) Average 1981–1998 seasonal cycle of $-Q_X$, SC[$-Q_X$]. (c) Seasonal and interannual variability of the 30-d running mean of $-Q_X$. (d) Deseasonalised cumulative sums of $-Q_X$ and the NAO index over the period 1981–1998, S[$-Q_X$] and S[NAO], respectively. Dashed line, 1-year running mean of S[$-Q_X$].

raw satellite passes were supplied by the NERC Satellite Receiving Station, Dundee, Scotland and processed following Miller, Groom, McManus, Selley, and Mironnet (1997). Briefly, the thermal infra-red channels were calibrated (Planet, 1988) and SST computed using the split window technique (McClain, Pichel, & Walton, 1985) with appropriate NOAA algorithms for each AVHRR instrument. Clouds were detected and masked using a series of tests on the visible and infra-red channels (Miller et al., 1997) and the images were then remapped onto a Mercator projection using orbital ephemeris and an automated adjustment method to correct for residual navigation errors (Bordes, Brunel, & Marsouin, 1992). To investigate seasonal, monthly and interannual variability for the period 1987–1999, monthly composite AVHRR SST data

were obtained from the NASA Pathfinder project (Vázquez, Hamilton, Van Tran, & Sumagaysay, 1994); these data are mapped onto an equal-angle projection giving a latitudinal and longitudinal resolution of 9.8 and 7.3 km at 42°N.

2.4.2. Ocean colour

Ocean colour data were obtained from the NASA Sea-viewing Wide Field-of-view Sensor (SeaWiFS) launched in August 1997, an operational instrument that has provided daily high resolution ~1.1 km coverage over the Iberian Peninsula. Individual passes were supplied in level 1 format by the Dundee Satellite Receiving Station and analysed using the SeaWiFS Automated Processing System (SeaAPS: Lavender & Groom, 1999). SeaAPS automatically applies NASA algorithms to perform calibration, navigation images and atmospheric correction (Gordon & Wang, 1994). Images of water leaving radiance are then used to compute chlorophyll concentration with the OC4 algorithm (O'Reilly et al., 1998) or combined to produce near-true colour images that can show scattering and absorption in the 555, 510 and 443 nm bands (Lavender & Groom, 1999). Finally, the SeaWiFS images are remapped to the same Mercator projection as the AVHRR data. SeaWiFS monthly composites on an equal-angle projection with 9.8/7.3 km pixel size (at 42°N) were obtained from the NASA Goddard Distributed Active Archive Center to investigate the monthly and interannual characteristics of chlorophyll in the study area.

2.5. Plankton counts and estimation of primary production from P–E curves

Plankton samples were collected from 3 to 8 depths in the upper 100 m and preserved in Lugol's iodine. The organisms were identified and counted to the species level where possible using an inverted microscope and composite sedimentation chambers. Small species (<20 μm) were counted along single transects at ×250 and ×400 magnification, and a scan of the whole slide at ×100 magnification was used for larger species. Inverted microscope counts cover the nano- (2–20 μm) and plankton (20–200 μm) size ranges, but the preservation procedure can result in losses in the nanoplankton fraction, which is mainly composed of flagellates. The picoplankton fraction (<2 μm) has not been included. The count data for GALICIA-XII and MORENA-I cruises provided information on horizontal distributions of plankton species, and vertical distribution data are available from selected transects (see Fig. 1) sampled during the GALICIA-XII, MORENA-II, CD110b, MORENA-I and Bg9815c cruises.

Photosynthesis–irradiance (P–E) relationships were determined at 3–5 depths in the water column during cruises GALICIA-XII, CD110b, MORENA-I and Bg9815c. Sampling depths were selected on the basis of the Chl-fluorescence profiles obtained with a fluorometer attached to the rosette sampler. Where a deep chlorophyll maximum (DCM) was observed, one sample was taken in the maximum, two samples from the upper and lower tails of the DCM, together with one sample from the surface and one sample from the depth of 1% PAR. The P–E experiments were conducted in linear incubators illuminated at the front by tungsten halogen lamps. Each incubator housed 14 subsamples held in 75 ml tissue culture Corning flasks, inoculated with 185 kBq (5 μCi) of ^{14}C-labelled bicarbonate. The incubators were cooled with circulating surface water. The photosynthetic available radiation (E_{PAR}) at the position of each incubation bottle was measured with a Li-Cor cosine sensor LI-190SA. The flask at the end of the incubator was covered with aluminium foil and used as a measure of dark fixation. After 2–3 h of incubation, samples were filtered through 25 mm glass fibre filters (Whatman GF/F) and were exposed to concentrated HCl fumes for 12 h. Radioactivity was determined using the external standard and the channel ratio methods to correct for quenching. The P–E parameters were estimated by fitting the data to the model of Platt, Gallegos, and Harrison (1980). Water column primary production was integrated to a depth equivalent to 0.1% of surface irradiance using the P–E parameters, the chlorophyll concentration in the water column, the daily incident light and the vertical attenuation coefficient. Incident sea surface photosynthetic active radiation (PAR 400–700 nm) was measured with a Li-Cor cosine sensor (LI-190SA) and light penetration

in the water column was determined using a Li-Cor spherical quantum sensor LI-193SA. Underwater PAR just below the sea surface was calculated by adjusting the PAR profile to the equation of light attenuation with depth. Light transmittance at the air–sea interface was calculated by dividing PAR light just below the sea surface by incident PAR at the sea surface.

3. Results and discussion

3.1. Wind-stress patterns off NW Spain

According to Bakun and Nelson (1991), during fall and winter the wind-stress curl near the NW coast of the Iberian Peninsula is low and irregular in its distribution, but becomes strongly cyclonic during spring and summer. Therefore, it is unlikely to be an important factor in the control of the onset of the PCCC, hence the simple wind-stress calculations in the 2° × 2° geostrophic cell centred at 43°N, 11°W (Fig. 1(c)) are considered sufficient to define the effects of the wind patterns on the seasonal reversals of the Portugal Coastal Current. Haynes and Barton (1990) observed that the weaker the equatorward wind-stress, the stronger the PCCC flow is, whereas a reversal of the PCCC flow only occurs if the equatorward wind-stress is sufficiently strong. Consequently, a quantitative study of the recurrent modes of temporal variation of $-Q_X$ will provide information on the effects of the expected hydrographic variability on event, seasonal and interannual time-scales. We first focus on seasonal variability (Section 3.1.1), then on interannual variability (Section 3.1.2), and finally on event scale variability (Section 3.1.3). The interannual variability of $-Q_X$ will be matched to AVHRR sea surface temperatures (SST) (January mean).

3.1.1. Seasonal variability: extension and intensity of the downwelling season

Retention of the first ($T = 365$ d) and second ($T = 183$ d) harmonics of a Fourier analysis applied to the complete 1981–1998 time series of $-Q_X$ values (Fig. 2(a)) produces the average seasonal cycle, SC$[-Q_X]$ (Fig. 2(b)), and reveals the two well-defined periods previously noted by Wooster et al. (1976). A upwelling-favourable season (equatorward wind-stress) extends from the beginning of April to the end of September and there is a seasonal maximum of $-Q_X$ of 0.4×10^3 m^3 s^{-1} km^{-1} in July. The downwelling-favourable season (poleward wind-stress) extends from the beginning of October to the end of March and there is a seasonal minimum of $-Q_X$ of -0.5×10^3 m^3 s^{-1} km^{-1} in December. The average duration and $-Q_X$ values for the 1981–1998 upwelling-favourable seasons were 188 d and 0.27×10^3 m^3 s^{-1} km^{-1}, respectively. The comparable averages for downwelling-favourable seasons were 177 d and -0.33×10^3 m^3 s^{-1} km^{-1}, respectively. Therefore, the average SC$[-Q_X]$ is slightly biased towards downwelling-favourable values. However, this parameter only retains 12% of the total variability of the 1981–1998 time series, which indicates that the seasonal signal is of relatively low intensity. The SC$[-Q_X]$ values calculated for each individual year retain from <5% in 1985–1986 to >27% in 1989–1990 of the total annual variability (Table 2).

The interannual variability of the monthly running mean of $-Q_X$ (Fig. 2(c)) indicates that there is high variation in the timing of the onset and the cessation of the downwelling-favourable season each year, and that downwelling events occur frequently during the upwelling season and vice versa. The onset of the downwelling-favourable season tended to occur regularly between mid-September and mid-October, but the timing of its cessation ranged from early February to late May. The onset of the downwelling-favourable season coincided with the 'autumn phytoplankton bloom' and the subsequent period of intense organic matter degradation characteristic of temperate ecosystems (Nogueira, Pérez, & Ríos, 1997). Whereas the timing of the cessation of the downwelling-favourable season overlapped with the period of the 'spring bloom' (Figueiras & Niell, 1987; Nogueira et al., 1997). The occurrence/absence of the PCCC at the time of the spring and autumn blooms has key implications for the fate of the fresh organic materials produced

Table 2
Distribution of the temporal variance of $-Q_X$ for different years throughout the 1981–1998 study period

Year (August–July)	SC[$-Q_X$] (%EV)		Short-term bands		Significant harmonics (%EV>5, $p < 0.05$)
	$T = 365$	$T = 183$	$30 \geq T > 7$	$7 \geq T \geq 2$	
1981–1982	9.6	2.1	30.8	29.4	46 (5.2), 19 (5.8)
1982–1983	3.4	6.5	39.7	29.9	24 (5.2)
1983–1984	7.1	0.4	34.0	33.0	20 (5.0)
1984–1985	12.8	0.2	25.5	34.9	61 (5.1), 52 (5.1)
1985–1986	3.2	1.5	31.5	35.4	30 (7.2)
1986–1987	10.4	0.2	28.9	50.0	–
1987–1988	8.5	3.2	34.0	35.8	–
1988–1989	11.6	1.8	34.9	38.7	–
1989–1990	19.9	7.3	31.2	28.3	–
1990–1991	8.9	1.2	36.9	32.7	16 (5.1)
1991–1992	5.2	4.3	38.5	31.7	17 (5.0), 13 (5.5)
1992–1993	4.3	3.8	27.4	33.0	73 (5.4), 61 (7.9), 30 (5.2)
1993–1994	5.4	×	31.2	43.5	×
1994–1995	13.5	3.7	33.5	33.3	91 (6.4), 24 (8.0)
1995–1996	12.3	5.6	30.4	26.6	91 (8.6), 73 (10.5)
1996–1997	10.0	1.2	31.8	33.2	121 (5.8)
1997–1998	7.7	4.2	42.2	31.4	21 (7.9)

Years are defined from August to July, such that the downwelling-favourable season is at the middle of each period. The percentage of explained variance (%EV) retained by the first ($T = 365$ d) and second ($T = 183$ d) harmonics of the annual period (which defines the seasonal cycle, SC[$-Q_X$]), and by the short-term bands of $T < 30$ d are indicated. The last column shows the period (%EV) of some significant harmonics, those with %EV>5% and $p < 0.05$, each year.

during these events in the coastal zone; i.e. in the balance between off-shelf export and in situ sedimentation. Of particular interest were the results from September 1991 (GALICIA-XII) cruise, when the coastal winds shifted from downwelling- to upwelling-favourable and the May 1993 (MORENA-I) cruise, when there was an isolated downwelling-favourable period lasting about a month.

3.1.2. Decadal change of $-Q_X$ and its effect on the development of the PCCC

In order to highlight any possible interannual variability in the $-Q_X$ time series, it was necessary to filter out the seasonal and event (high frequency) components (Fedorov & Ostrovskii, 1986). The seasonal component was removed by subtracting the average SC[$-Q_X$] for 1981–1998 (Fig. 2(b)) and the event component by the cumulative sums method (Ibanez et al., 1993). The corresponding cumulative function $S[-Q_X]$ (Fig. 2(d)) is

$$S[-Q_X(t)] = (-Q_X(t) - \mathrm{SC}[-Q_X]) + S[-Q_X(t-1)], \quad (2)$$

where t is time in Julian days. The lower $S[-Q_X]$ values indicate preferred wind conditions for PCCC development off the NW Iberian Peninsula. A negative (positive) trend in $S[-Q_X]$ indicates transition to PCCC-favourable (unfavourable) periods.

$S[-Q_X]$ from Fig. 2(d) appears to indicate a long-term cycle with a periodicity T~10 years; minimum values (PCCC favourable) occurred during the mid-1980s (1984–1986) and maximum values (PCCC unfavourable) in the mid-1990s (1994–1996). An abrupt $S[-Q_X]$ trough occurred in 1983 when there was a marked minimum in late autumn, indicating that the SC[$-Q_X$] had shifted strongly towards downwelling

conditions (Fig. 2(c)). This observation is consistent with Pingree and Le Cann (1989), who identified a marked warming along the north Spanish coast in the beginning of 1984. The GALICIA-VI and GALICIA-VII cruises took place in December 1983 and February–March 1984, respectively, allowing us to define the PCCC during a particularly favourable year. Wind-stress patterns in 1985 and 1989 were also exceptionally favourable to the development of PCCC, and this was reflected in the amplitude of the seasonal signal during the downwelling season 1989–1990, when several $-Q_X$ minima below -1.0×10^3 m^3 s^{-1} km^{-1} were observed (Fig. 2(c)). In contrast, the wind patterns during 1990 were particularly unfavourable for PCCC development, and only a brief trough in $S[-Q_X]$ was observed during the autumn. Pathfinder SST data for each January between 1987 and 1999 are shown in Fig. 3. The PCCC between 42° and 44°N is evident as a warming in most years, usually extending well into the Bay of Biscay in particular during 1990 (and 1996), but with notable exceptions in 1991 (and 1994). Hence, the exceptionally warm temperature anomaly (+1.5 °C in the ENACW domain) recorded by Pingree (1994) in January 1990 in the southern Bay of Biscay can be attributed at least in part to the warm PCCC observed off Northern Spain in the winter of 1989–1990. Pingree also indicated that there is little evidence for the presence of a marked PCCC in the winter of 1990–1991. A marked (brief) trough on $S[-Q_X]$ was observed in 1995 (1993).

Although $S[-Q_X]$ during the years 1991, 1992 and 1993 was not particularly favourable for the development of the PCCC, this feature was observed during cruises GALICIA-XII (September 1991), MORENA-I (May 1993) and MORENA-II (November–December 1993) (see later). Under these conditions, wind-stress helps to modulate the intensity of the PCCC, which is induced primarily by geostrophic adjustment of the weak eastward oceanic flow driven by the large-scale meridional baroclinic pressure gradient (Frouin et al., 1990). In this sense, Fig. 3 also shows the average SSTs each January for the slope region influenced by the PCCC in an area delineated by 42° and 43°N, and 9.5° and 10°W. The SST variations correlate well with SST data from along the continental slope north of Spain between 4° and 8°W (see the 'Centre de Meteorologie Spatiale/Centre de Meteorologie Marine' data presented in Pingree (1994) in his Fig. 2 during 1987–1993). This is not surprising since a strong PCCC warming on the slope west of Spain is also likely to be reflected in warming along the north coast. However, a stronger warming does not necessarily mean a stronger PCCC since the PCCC SST correlates well with average SST in an offshore region (42°–43°N; 11°–13°W; Fig. 3) suggesting that either the interannual temperature variations are caused by larger scale forcing or that the poleward flow induced by the pressure gradient affects a much broader region.

Wind patterns changed completely during the second half of the 1990s, when both the intensity and duration of the downwelling season increased. The abrupt trough on $S[-Q_X]$ during 1997 demonstrates that conditions were especially favourable for the development of the PCCC, hence the marked warm water flow seen in January 1998, during cruise CD110b. Finally, a close coupling between the long-term components of a basin-scale index such as the 'North Atlantic Oscillation' (S[NAO]) and a meso-scale index (2° × 2°) such as $-Q_X$ ($S[-Q_X]$) is clearly observed in Fig. 2(c).

3.1.3. Event scale variability

It must be emphasised that most of the variability in the $-Q_X$ time series is associated with the short-term bands of period ≤30 d (Table 2). The contribution of these events to the total variability averaged 66% during 1981–1998, and ranged from a minimum of 57% in 1995–1996, to a maximum of 79% in 1986–1987. A significant amount of this event scale variability (>5%, $p < 0.05$) occurred as single modes of variation with periods in the range 13–30 d (Table 2). This event scale periodicity is a characteristic feature of the NW Spain upwelling system (Álvarez-Salgado, Rosón, Pérez, & Pazos, 1993; Blanton et al., 1987). However, it should also be noted that significant modes of longer period such as 1/6 (61 d), 1/5 (73 d), 1/4 (91 d) and 1/3 (121 d) of the annual period were also apparent in certain years.

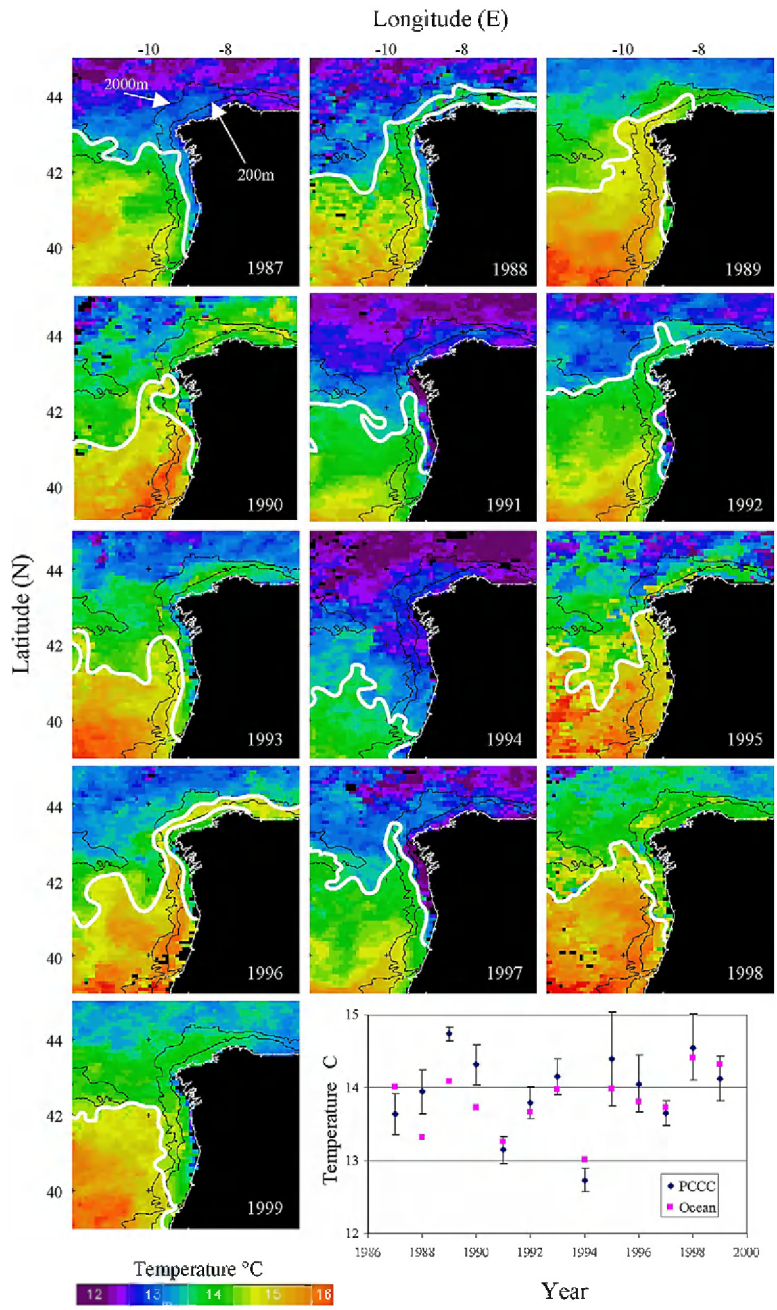

Fig. 3. AVHRR pathfinder 9-km resolution sea-surface temperature images for each January from 1987 to 1999 (monthly composite). The 200 and 2000 m depth contours are marked on each image. The white lines represent the boundaries of the PCCC. Bottom right panel: extracted mean SST for a PCCC 'box' 42°–43°N; 9.5°–10°W (±SD) and ocean box 42°–43°N; 11°–13°W (SD omitted for clarity).

3.2. A physical framework for the PCCC off NW Spain

Geopotential anomaly, temperature and salinity distributions have been analysed along this section with the aim of setting the framework necessary to appreciate the chemical and biological features generated by the PCCC off NW Spain (42°–43°N) rather than to contribute further to our already profuse knowledge on the physics of this feature. The distributions allow us to examine the geostrophic velocity fields (Section 3.2.1) and the geometry (Section 3.2.2) of the PCCC—defined by the convergence and divergence fronts observed from the satellite images—under the contrasting conditions observed during the seven cruises. In addition, we describe for the first time a marked seasonal cycle in stratification/mixing in the PCCC domain (Section 3.2.3).

3.2.1. Intensity of the PCCC deduced from the geopotential anomaly fields

The September 1991 cruise was carried out at the time of the autumn transition from upwelling- to downwelling-favourable coastal winds. The monthly running mean of $-Q_X$ (Fig. 2(c)) indicates that the cruise occurred during a low wind-stress period ($-Q_X = +90 \pm 50$ m^3 s^{-1} km^{-1}) after weak downwelling-favourable winds during the previous week. At the start of the cruise, winds (ship measurements) were from the west (stations 11–65; average 4.5 m s^{-1}) but by the end of the cruise they had swung round to a northerly direction (stations 71–85; average 5 m s^{-1}). As a result of the variable wind pattern, the geopotential anomaly at 10 dbar (Fig. 4(a)) was patchy, varying from poleward flow off the northern coast, to equatorward flow off the western coast, and to off-shelf flow adjacent to the transitional Cape Finisterre transect (43°N). Geostrophic surface flows along a transect (stations 81–85, Fig. 1) were very weak and southerly over the shelf (2 cm s^{-1}) but slightly stronger at the slope (4.5 cm s^{-1}), which was consistent with hydrographic conditions expected for a transitional wind-calm period at the time of the onset of the PCCC.

PCCC-favourable southerly wind conditions ($-Q_X < 0$) prevailed during the late autumn (December 1983 and November–December 1993) and early winter (January 1998) cruises (Fig. 2(c)). The winds (ship measurements) during the December 1983 were from a southerly quarter with average speed of 6.2 m s^{-1}. Strong northerly geostrophic surface currents were observed across the southernmost transect from 11°W (−11°E) to the coast, with average and maximum velocities of 4 and 10 cm s^{-1}, respectively. The PCCC current narrows in the vicinity of Cape Finisterre where it has maximum geostrophic velocities of 10 cm s^{-1} (Fig. 4(b)). In contrast, a weak (average speed, 3 cm s^{-1}) southward flowing current (the Portugal current) is observed in the northwestern corner of the domain sampled in December 1983 (stations 7 and 10). Similar values were calculated by Frouin et al. (1990) along 42°N during the MEDPOR/2 cruise (November 29–December 6, 1983). The winds during the November–December 1993 cruise averaged 7.0 m s^{-1} and so were also PCCC favourable, and a poleward geostrophic current of average speed 6 cm s^{-1} was observed east of 10°W (−10°E) along 41°45′N (Fig. 4(c)). As observed during the December 1983 cruise, the current narrowed towards the north. It is to be noted that during this cruise the zonal entry of oceanic waters at 41°N marked by the 4.0 m^2 s^{-2} isoline. Strong southerly winds (average 15 m s^{-1}) were experienced during the January 1998 cruise, which restricted sampling to only five stations (Fig. 1). However, these still enabled the identification of a strong poleward geostrophic current of about 13 cm s^{-1} on the shelf (Fig. 4(d)).

As noted above (Section 3.1) the late winter cruise (February–March 1984) coincided with a period of upwelling-favourable winds during the downwelling season. The average (±SD) monthly running mean of $-Q_X$ was 185 ± 160 m^3 s^{-1} km^{-1}, while the mean wind velocity during the cruise was 8.2 m s^{-1}, from the northeast. Consequently, weak northeasterly geostrophic currents with maximum velocities of 2.5 cm s^{-1} dominated the study area (Fig. 4(e)). These conditions can be compared with the monthly running mean of $-Q_X$ (190 ± 100 m^3 s^{-1} km^{-1}; Fig. 2(c)) and the prevailing PCCC-favourable winds (southwesterly, average speed 6.3 m s^{-1}) experienced during the spring cruise in May 1993. The surface

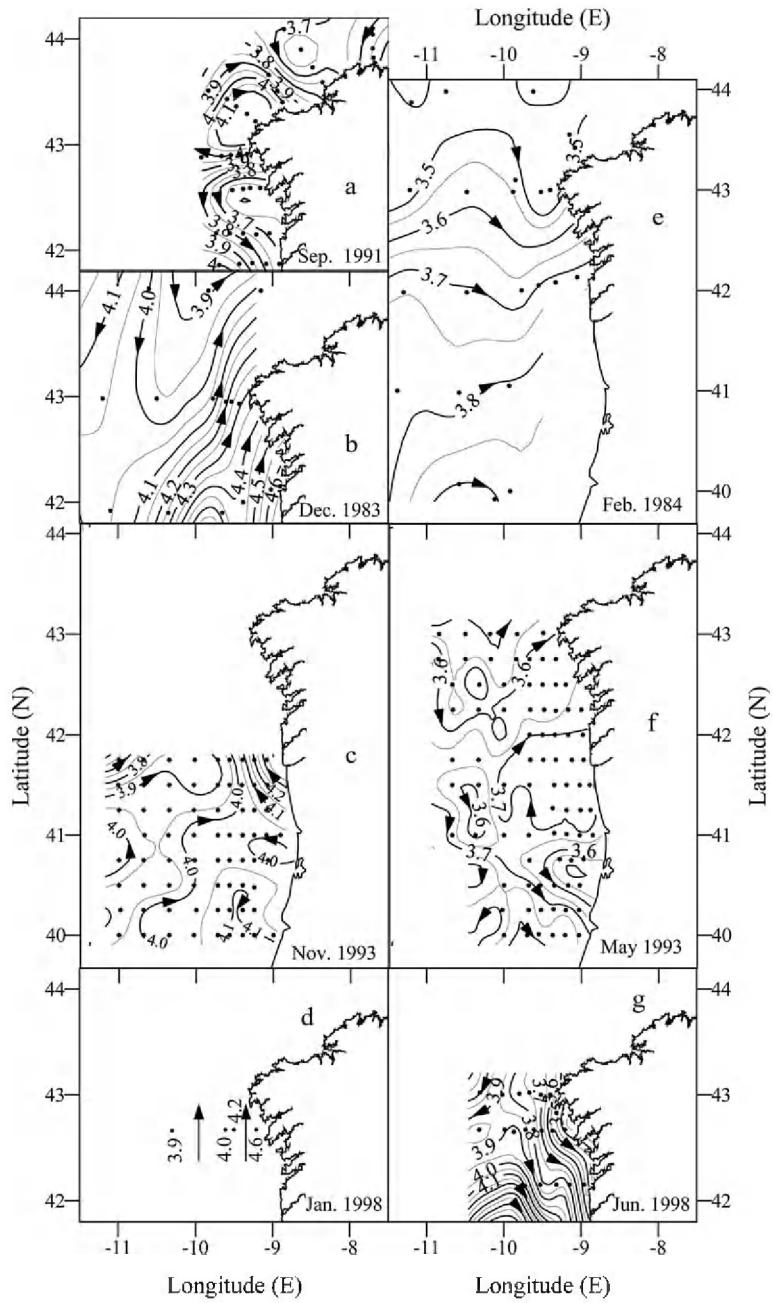

Fig. 4. Horizontal distributions of surface dynamic height (in $m^2\ s^{-2}$) referred to 350 dbar during the GALICIA-XII (September 1991) (a), GALICIA-VI (November–December 1983) (b), MORENA-II (November 1993) (c), CD110b (January 1998) (d), GALICIA-VII (February–March 1984) (e), MORENA-I (May 1993) (f), and Bg9815c (July 1998) (g) cruises. Superimposed on Fig. 5(c) is the conversion of distance among consecutive dynamic height isolines (separated 0.05 $m^2\ s^{-2}$) into geostrophic velocity (cm s^{-1}).

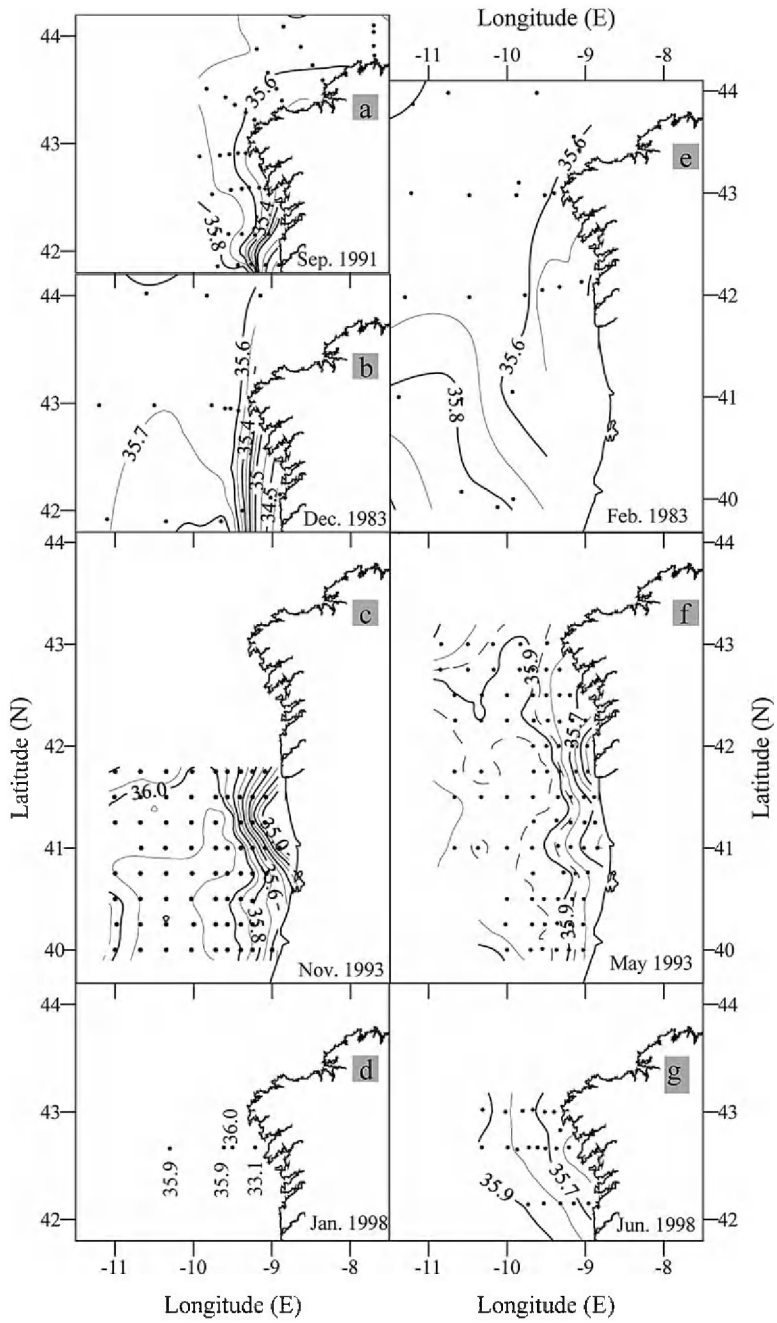

Fig. 5. Horizontal distributions of surface salinity during the GALICIA-XII (September 1991) (a), GALICIA-VI (November–December 1983) (b), MORENA-II (November 1993) (c), CD110b (January 1998) (d), GALICIA-VII (February–March 1984) (e), MORENA-I (May 1993) (f), and Bg9815c (July 1998) (g) cruises.

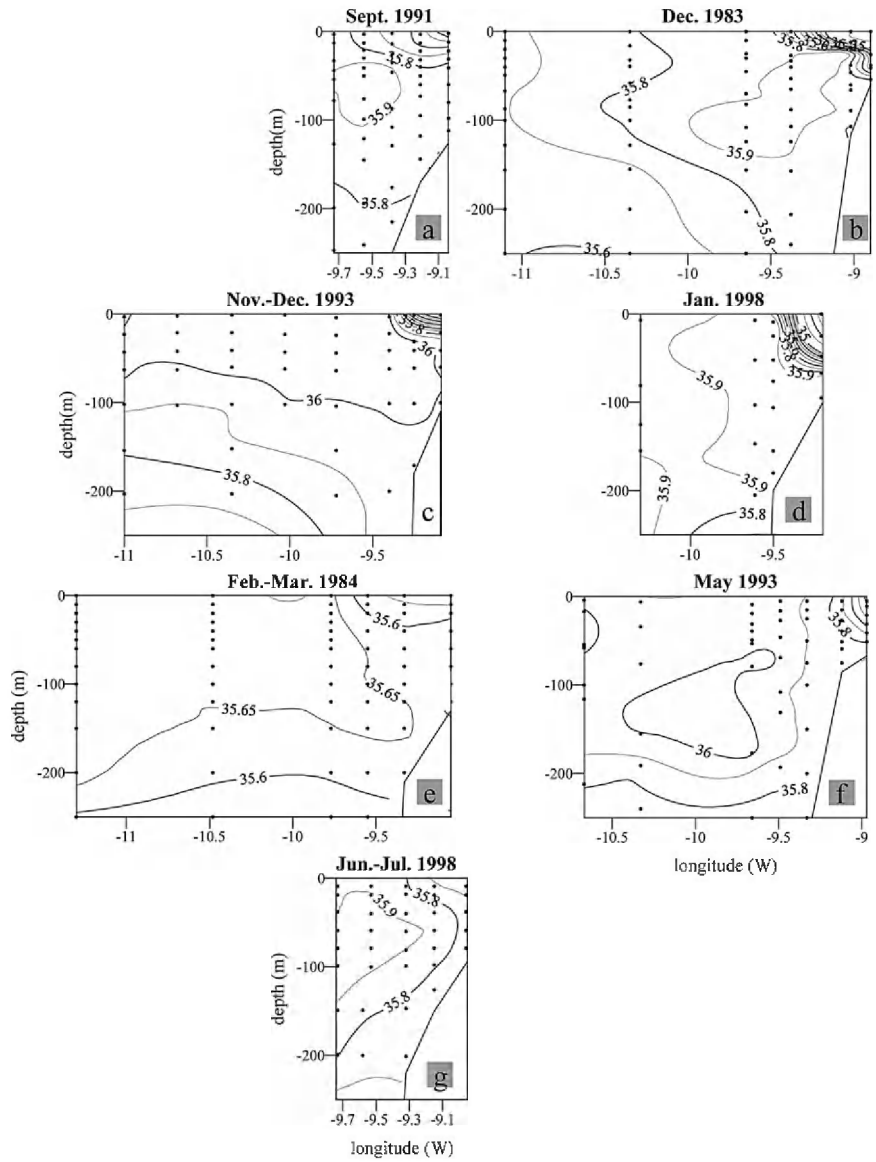

Fig. 6. Vertical distributions of salinity along the zonal lines indicated in Fig. 1 during the GALICIA-XII (September 1991) (a), GALICIA-VI (November–December 1983) (b), MORENA-II (November 1993) (c), CD110b (January 1998) (d), GALICIA-VII (February–March 1984) (e), MORENA-I (May 1993) (f), and Bg9815c (July 1998) (g) cruises.

geostrophic flow (Fig. 4(f)) clearly shows the zonal entry of the PCCC at 41°N and its northeastward progression, with a mean velocity of 2.5 cm s^{-1} near Cape Finisterre. A weak signal of the Portugal Current is also seen offshore in the northwest corner of the sampling area where there were southward geostrophic velocities of ~1 cm s^{-1}. The PCCC was also observed during April 1982 (McLain, Chao, Atkinson, Blanton, & de Castillejo, 1986), April 1987 (Bode et al., 1990), May 1989 (Mazé et al., 1997) and May 1993 (Fiúza et al., 1998). Therefore, the presence of the PCCC off Portugal and NW Spain during the spring appears to be a predominant hydrographic feature.

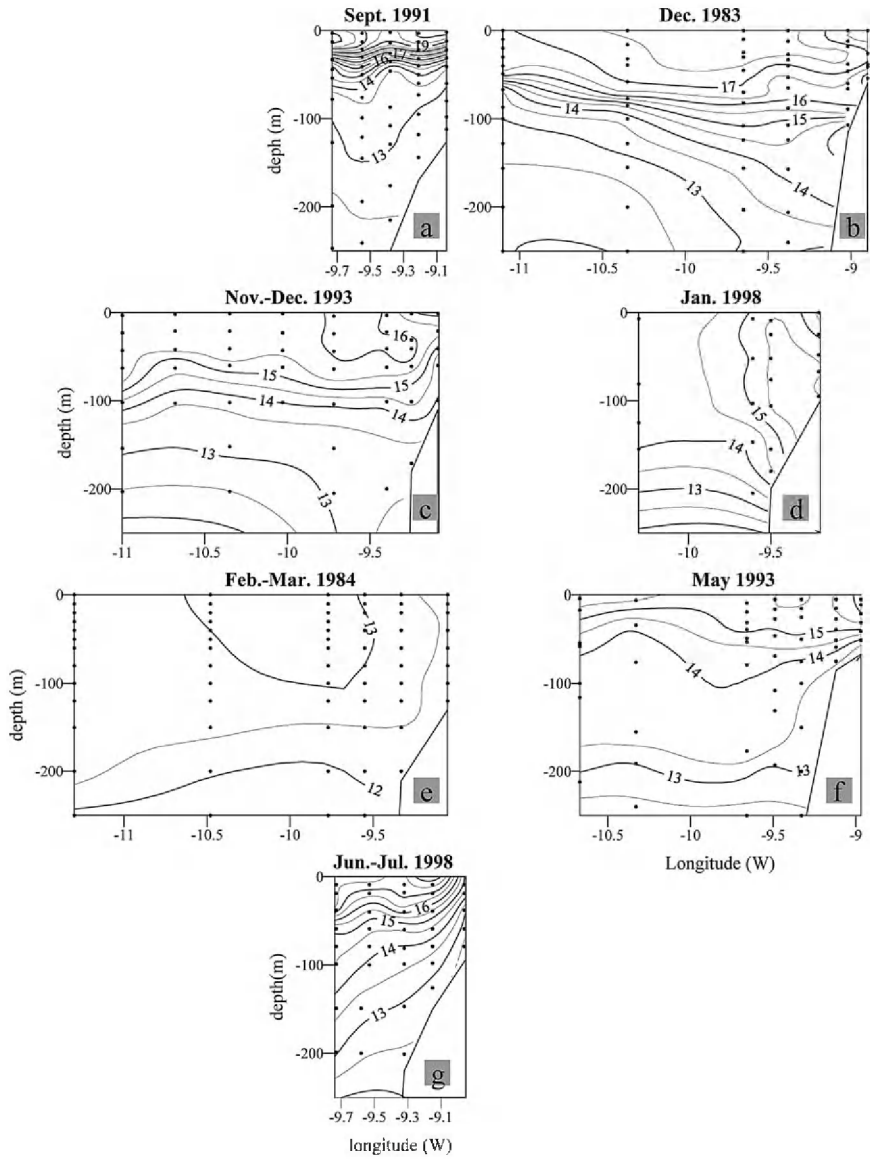

Fig. 7. Vertical distributions of potential temperature (°C) along the zonal lines indicated in Fig. 1 during the GALICIA-XII (September 1991) (a), GALICIA-VI (November–December 1983) (b), MORENA-II (November 1993) (c), CD110b (January 1998) (d), GALICIA-VII (February–March 1984) (e), MORENA-I (May 1993) (f), and Bg9815c (July 1998) (g) cruises.

As expected, during the summer cruise in June–July 1998, meteorological and hydrographic conditions were very different. The average (±SD) monthly mean of $-Q_X$ was 390 ± 40 $m^3\ s^{-1}\ km^{-1}$ with an average wind velocity during the cruise of 12 m s^{-1} from the northeast, these conditions being typical of steady and strong upwelling. Accordingly, geostrophic flow calculations (Fig. 4(g)) indicated strong southward geostrophic currents, with an average southward velocity of 5 cm s^{-1} in the study area and maximum values of ~10 cm s^{-1} along 42° 9′N, off Ría de Vigo.

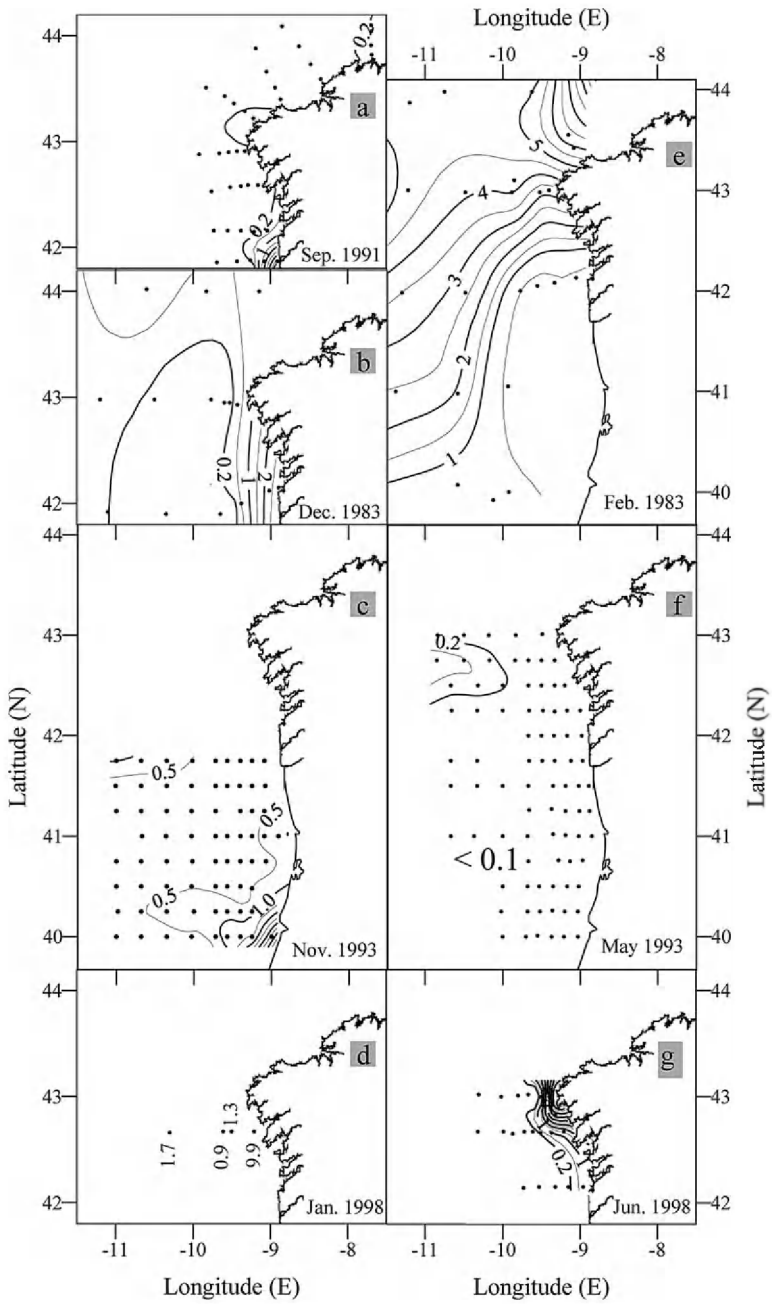

Fig. 8. Horizontal distributions of surface nitrate (μmol kg^{-1}) during the GALICIA-XII (September 1991) (a), GALICIA-VI (November–December 1983) (b), MORENA-II (November 1993) (c), CD110b (January 1998) (d), GALICIA-VII (February–March 1984) (e), MORENA-I (May 1993) (f), and Bg9815c (July 1998) (g) cruises.

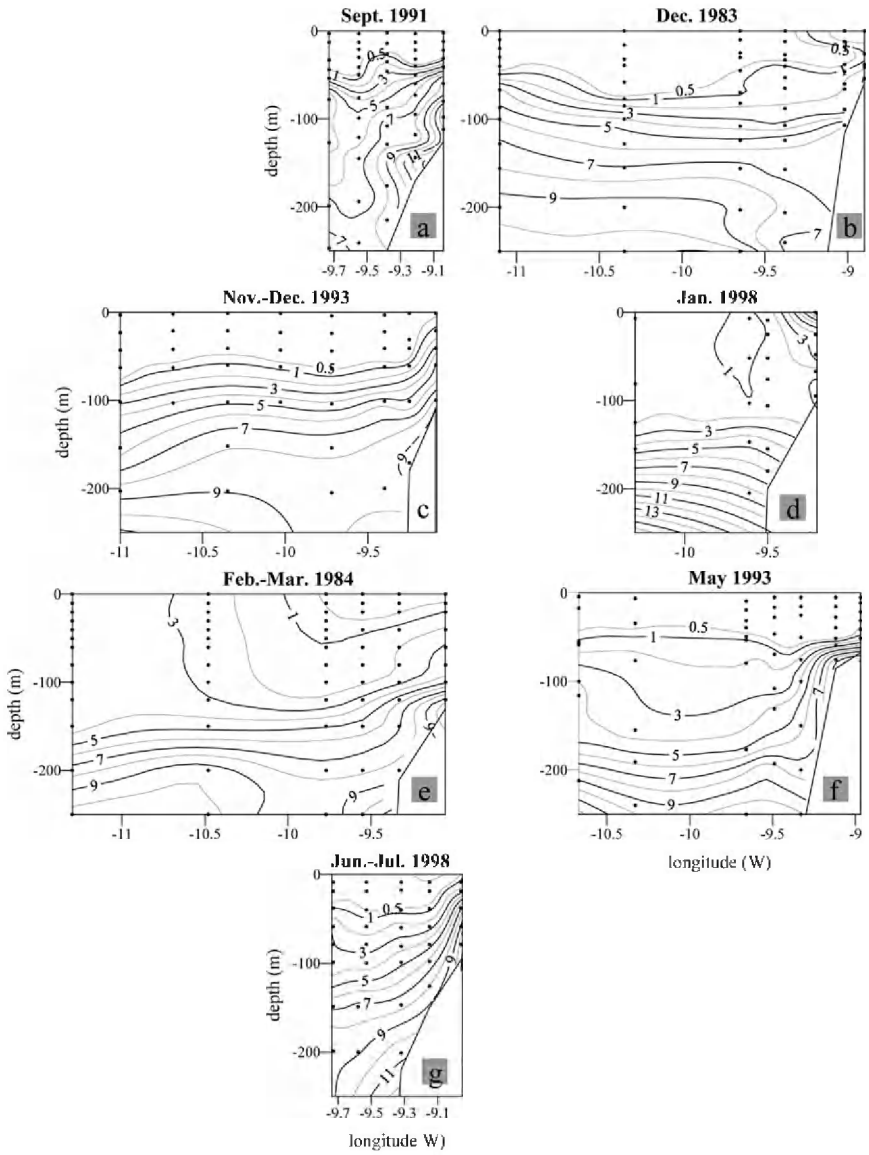

Fig. 9. Vertical distributions of nitrate (μmol kg^{-1}) along the zonal lines indicated in Fig. 1 during the GALICIA-XII (September 1991) (a), GALICIA-VI (November–December 1983) (b), MORENA-II (November 1993) (c), CD110b (January 1998) (d), GALICIA-VII (February–March 1984) (e), MORENA-I (May 1993) (f), and Bg9815c (July 1998) (g) cruises.

3.2.2. Oceanic and coastal boundaries of the PCCC

The presence of poleward flowing slope currents along oceanic eastern boundaries is usually accompanied by a clear thermohaline signal resulting from the transport of anomalously warm and salty waters (Mooers, 1989). In our case, the PCCC was conveying surface and central waters of subtropical origin ($\sigma_0 <$ 27.0 kg m^{-3}) into the study region. In both the AVHRR images (Fig. 1) and the horizontal distributions of surface salinities (Fig. 5) the PCCC shows up as an elongated core of high temperature and high salinity water in the CTZ off the NW Iberian Peninsula.

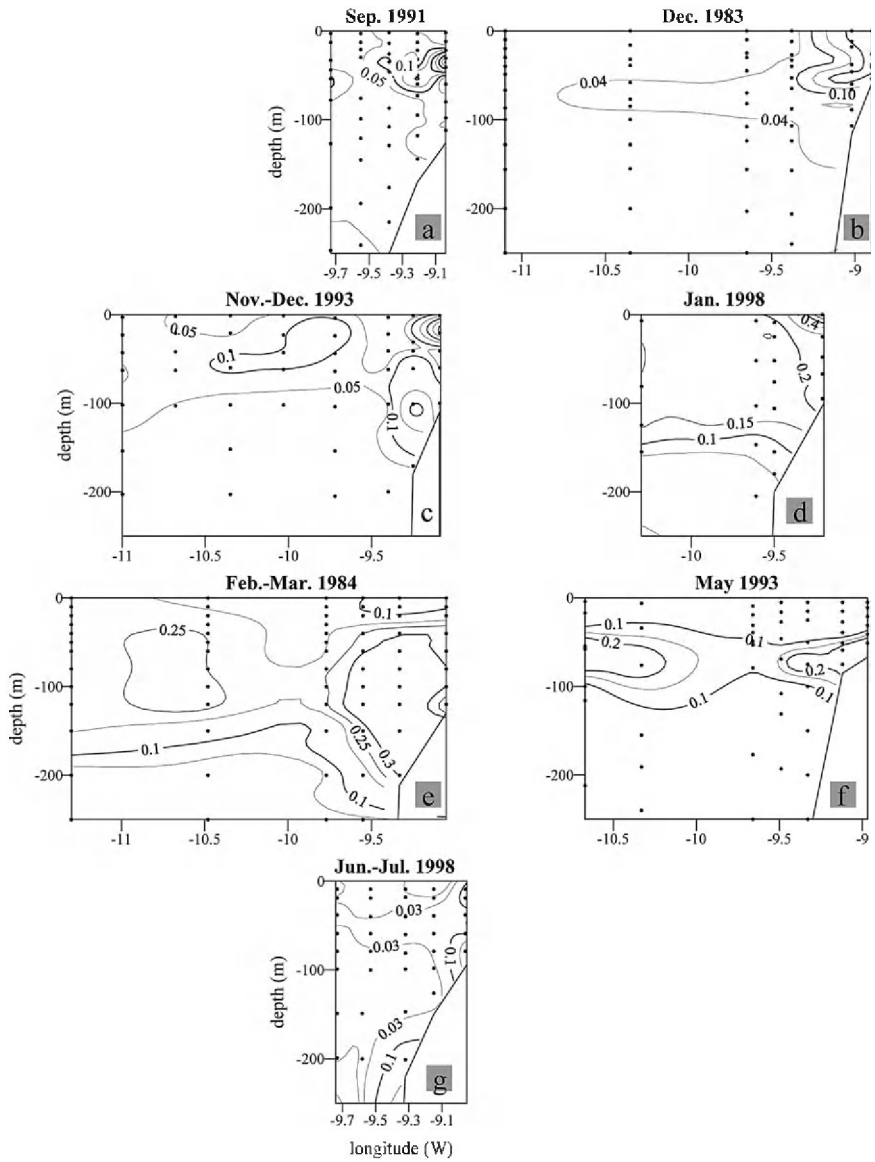

Fig. 10. Vertical distributions of nitrite (μmol kg^{-1}) along the zonal lines indicated in Fig. 1 during the GALICIA-XII (September 1991) (a), GALICIA-VI (November–December 1983) (b), MORENA-II (November 1993) (c), CD110b (January 1998) (d), GALICIA-VII (February–March 1984) (e), MORENA-I (May 1993) (f), and Bg9815c (July 1998) (g) cruises.

Satellite imagery (Fig. 3) indicates that there were thermal fronts at the coastal and oceanic boundaries of the PCCC. A band, or patches, of cool water adjacent to the west coast was separated from the warmer PCCC waters over the continental slope by a clear convergence front. There is, however, interannual variability and clearly defined fronts that occurred only in 1987, 1990, 1991, 1996, and 1997. In other years there were either only small patches of cool water, as in 1992, or there was a complete absence of cool surface water, as in 1989 at 42°N. The front accumulates low salinity and cool waters on the shelf originating from the discharge from the Rías Baixas, which are four large coastal inlets of NW Spain that

receive continental waters from a 7×10^3 km^2 drainage basin (Fig. 1). In 1987–1996 average seasonal cycle of continental runoff to the Rías Baixas increased from 35 l s^{-1} km^{-2} in September to 70 l s^{-1} km^{-2} in November followed by a decrease to 63 l s^{-1} km^{-2} in January and 40 l s^{-1} km^{-2} in May (Nogueira et al., 1997). In agreement with the seasonal pattern of riverine discharge, the salinity gradient is especially pronounced during late autumn and early winter (Fig. 5(d)). During the early autumn (September 1991; Fig. 5(a)) and spring (May 1993; Fig. 5(f)), the inshore salinity gradient had become less pronounced and the front then appeared along the shelf break, apparently strongly related to the bottom topography (Bode et al., 1990; Fiúza et al., 1998; Haynes & Barton, 1990). The coastal band of cool water (Fig. 1) develops in late autumn, when the whole water column begins to cool as a result of net heat loss from the surface (Fiúza, 1984; Pérez et al., 1998). The coastward penetration of the PCCC depends on the relative intensity of shelf winds and intensity of the local continental runoff that activates the residual circulation pattern of the Rías Baixas. A recent study by Álvarez-Salgado, Gago, Miguez, Gilcoto, and Pérez (2000) demonstrates that penetration of PCCC waters into the Rías Baixas occurs when $Q_X/R \geq 7(\pm 2)$, with Q_X in units of m^3 s^{-1} km^{-1} and R (continental runoff) in units of m^3 s^{-1}.

The oceanwards boundary of the PCCC is characterised by a more diffuse divergence front that separates the subtropical water associated with the PCCC from the fresher and cooler open ocean water coming from the north. This outer front is apparent in the AVHRR SST images (Fig. 1) and in the horizontal distributions of salinity in the NW corner of the survey box for the December 1983, February–March 1984, May 1993 and November–December 1993 cruises (Fig. 5(b), (c), (e) and (f)).

Comparison of Fig. 5(b) (December 1983) and Fig. 5(e) (February–March 1984) indicates that the poleward flow was stronger and better-defined in December (SSS $>$ 35.7 at 42°–43°N) than in February (SSS $<$ 35.7). This anomaly is probably related to the stratification and the dominance of strong southerly winds in December 1983 whereas in February–March 1984 the stratification had overturned and winter mixed conditions and weak northerly winds prevailed, as reflected in the geopotential anomaly fields (Fig. 5(b) and (e)). There were also differences in the poleward flows between May 1993 (Fig. 5(f)) and November–December 1993 (Fig. 5(c)). The high salinity core of the PCCC had penetrated from offshore near 41°N during the late spring cruise, but during the late autumn cruise there were two branches of the PCCC: a northeastward flowing branch, which was also observed during the spring cruise (at 41°N), and a northward flowing branch on the southern side of the study area (at 40°N). This double structure is consistent with the calculated geostrophic flows (Fig. 4(c) and (f)) and is indicative of a southward displacement of the origin of the PCCC as the year progresses (Álvarez-Salgado et al., 1993).

3.2.3. Vertical structure of the PCCC: a seasonal cycle of stratification/mixing

A subsurface high salinity (>35.9) core centred around a depth of 50–100 m was observed at the slope stations during the early autumn (September 1991; Fig. 6(a)), late autumn (December 1983 and November–December 1993; Fig. 6(b) and (c)), late spring (May 1993; Fig. 6(f)) and summer (June–July 1998; Fig. 6(g)). A corresponding V-shape of the isotherms occurs in the vicinity of the high salinity core during the periods of the onset (Fig. 7(a)) and cessation (Fig. 7(f)) of the PCCC. The presence of the core during the early autumn is a consequence of the transitional upwelling/downwelling-favourable conditions recurrently observed at these particular times and indicates the presence of previously upwelled ENACW over the shelf, where it is confined by the PCCC. During the downwelling-favourable late autumn and early winter cruises (Fig. 7(b), (c) and (d)) the isotherms slope downwards in the onshore direction, intercepting the bottom at the shelf break. The same structure is retained during the slightly upwelling-favourable late winter cruise (Fig. 7(e)) and reflects at depth the corresponding convergence front between coastal and PCCC waters observed in the surface layer. During the summer cruise, the isotherms sloped upwards in the inshore direction (Fig. 7(g)), indicating vigorous upwelling of ENACW with the high salinity core (Fig. 6(g)) tracing the northward displacement of the summer Portugal Coastal Undercurrent (Batteen, Martinez, Bryan, & Buch, 2000).

The subsurface salinity maximum develops in late spring, when a very shallow thermocline overlies the deeper remnants of the saltier mixed layer of ENACW from the previous winter (Fiúza et al., 1998). At this time, the salinity difference between the surface and the high salinity core is <0.1 (Fig. 6(f)). The high salinity core is maintained beneath the seasonal thermocline during the summer (Fig. 6(g)) and early autumn (Fig. 6(a)) and surfaces from late autumn to late winter in the PCCC domain (Fig. 7(c), (d) and (e)), in tandem with the increased mixing conditions in the surface layer. Thus, the upper mixed layer depth in the PCCC domain progressively increases from 20 m in early autumn (with maximum surface temperatures >20 °C), to 60 m in late autumn (SST > 15.5 °C), to 125 m in early winter (SST < 15 °C) and to 150 m in late winter (SST < 14 °C). The situation in December 1983 (Figs. 6(b) and 7(b)) was exceptional, with temperatures >17 °C over the upper mixed layer and a marked subsurface salinity maximum, in sharp contrast with the observation of a temperature of 15 °C over the 60 m thick mixed layer in November 1993. As indicated in Section 3.1, the wind field in 1983–1984 was especially favourable for the development of the PCCC, while it was unfavourable in 1993–1994 (Fig. 2(d)).

3.3. New insights on the effects of the PCCC on the distributions of chemical parameters

Horizontal and vertical distributions of selected chemical tracers show the imprint of the PCCC in the coastal, transitional and oceanic waters off NW Spain. The domain of the PCCC is characterised by low surface nutrient concentrations relative to the surrounding coastal and oceanic waters. Relatively high carbon and nutrients and low oxygen concentrations were observed in the ENACW domain as a consequence of oceanic mineralisation (Section 3.3.1) and nitrite is revealed as a tracer of stratification/mixing conditions and associated trophic status of the PCCC (Section 3.3.2).

The convergence front between the PCCC and coastal waters results in a reduction of the off-shelf export of primary production, and so enhances in situ sedimentation and pelagic/benthic mineralisation processes on the shelf which, in turn, affects carbon, nutrient and oxygen distributions. In contrast, the local upwelling along the divergent front between the PCCC and the surrounding oceanic water enhances vertical fluxes of nutrients to the nitrogen-exhausted surface layer. Nutrient enrichment of shelf bottom waters has been discussed by Álvarez-Salgado et al. (1997), Álvarez-Salgado et al. (1993), and Prego and Bao (1997), hence here we only illustrate the vertical distributions of NO_3^- (Fig. 9) to indicate the substantial nutrient enrichment in shelf bottom waters relative to ENACW of the same temperature in the surrounding ocean. This contrast was especially intense during the onset (Fig. 9(a)) of the PCCC, when there was an increase in nitrate concentrations in 13–13.5 °C water from <7 μmol kg^{-1} in the ocean domain to >11 μmol kg^{-1} over the shelf. Nutrient enrichment in bottom shelf waters was also marked during the late autumn cruise (November–December 1993; Fig. 9(c)), the late winter cruise (February–March 1984; Fig. 9(e)) and during the cessation of the PCCC (May 1993; Fig. 9(f)). In contrast, nutrient-poor PCCC waters occupied the bottom inner shelf during January 1998 (Fig. 9(d)). During June–July 1998 the parallel configuration between temperature (Fig. 7(g)) and NO_3^- profiles (Fig. 9(g)) indicates that there was a reduction in the nutrient enrichment during strong upwelling event.

Horizontal distributions of NO_3^- (Fig. 8) show relatively high nutrient concentrations in the surface layer of the coastal domain during the late autumn (December 1983) and early winter (January 1998) cruises as a result of the accumulation of the nutrient-rich, low salinity (Figs. 5 and 6) continental waters then being discharged from the Rías Baixas (Pérez, Álvarez-Salgado, Rosón, & Ríos, 1992). Surface nutrients in the coastal domain were very low (<0.2 μmol kg^{-1} NO_3^-) during both the onset (September 1991; Fig. 8(a)) and cessation phases (May 1993; Fig. 8(f)) of the PCCC. Whereas the enhanced nutrient concentrations observed on the southern side of the coastal domain during the November–December 1993 cruise (Fig. 8(c)) resulted from intense vertical mixing and entrainment of nutrient-rich deeper waters rather than from land runoff, as indicated by the high salinity of the surface waters (Fig. 5(c)) and the homogeneous vertical profiles of the thermohaline and of the chemical tracers at stations 72 and 73 (not shown).

High surface nutrient concentrations observed during the summer cruise (June–July 1998), mainly in the Cape Finisterre area (>6 μmol kg^{-1} NO_3^-), were a result of upwelling, as indicated by the low SST in the coastal domain (Fig. 1). The vertical NO_3^- profiles (Fig. 9) support this conclusion. It is remarkable also that the weak salinity stratification of coastal waters observed during the February–March 1984 cruise (Fig. 6(e)) kept NO_3^- concentrations below those recorded in the vigorously mixed PCCC and oceanic waters (Fig. 9(e)).

3.3.1. Chemistry of surface and central waters transported by the PCCC

The principal attribute of the subtropical surface waters transported by the PCCC to the Eastern North Atlantic temperate/subpolar transition area is their lower nutrient concentrations relative to both the adjacent coastal and oceanic waters. This is clearly shown in the surface (Fig. 8) and vertical (Fig. 9) distributions of NO_3^-. The effect on nutrient distributions of the divergent front in juxtaposition to the oceanic waters is clearly evident in the relatively high surface nutrients in the NW corner of the November–December 1993 (Fig. 8(c)) and May 1993 (Fig. 8(f)) cruises. In the PCCC domain, surface NO_3^- concentrations were usually <0.5 μmol kg^{-1}, except during the period when winter mixing deepened the mixed layer to 125–150 m when concentrations rose to 1.5–2.0 μmol kg^{-1}. For comparison, surface NO_3^- concentrations were >4 μmol kg^{-1} in the oceanic domain west of the PCCC flow. These low NO_3^- values in the surface waters of the PCCC have important implications for the extension of the spring bloom. Assuming a Chl-*a* production to NO_3^- consumption ratio of 1:1 (the theoretical maximum for phytoplankton of Redfield composition; Anderson, 1995), Chl-*a* levels at the time of the spring bloom will never exceed 2 mg m^{-3} in the PCCC domain. Evidence supporting this comes from the SeaWiFS monthly composites for 1998, 1999 and 2000 (not shown): in the region influenced by the PCCC (40.5°–41.5°N, 9.5°–11°W) the spring chlorophyll maximum is ~1 mg m^{-3}. Since HPO_4^{2-} and SiO_4H_4 excesses of 0.03–0.04 and 0.5–1.5 μmol kg^{-1}, respectively, were maintained in waters with NO_3^- <0.1 μmol kg^{-1} (not shown), it seems that nitrogen is the limiting nutrient for primary production in surface PCCC waters.

AOU can be used as an indicator of the balance of physical (net exchange across the air–sea interface) and biogeochemical (production/mineralisation) processes operating in surface PCCC waters. Primary production is the dominant process contributing to AOU during the onset of the PCCC (September 1991 cruise), inducing average AOU values of −10 μmol kg^{-1} (not shown), whereas in the coastal domain AOU was of the order of −40 μmol kg^{-1}. These numbers agree with the primary production rates recorded during the September 1991 cruise, which were 4–6 times higher in the coastal than in the PCCC domain (Section 3.4.3). Oxygen concentrations in PCCC waters were in equilibrium with the atmosphere (−1.0 < AOU < 2.0 μmol kg^{-1}) during the late autumn and early winter cruises, most probably because of the low primary production (Section 3.4.3) and enhanced air-sea exchange (intense coastal winds, Section 2.2). At this time, slight regeneration was observed in the coastal domain, where the average AOU was +8 μmol kg^{-1}. During the late winter cruise, weak mineralisation dominated in the PCCC domain (average AOU, +4 μmol kg^{-1}) but intense primary production occurred in the coastal domain (average AOU, −30 μmol kg^{-1}), suggesting that the onset of the spring bloom had taken place in coastal waters off NW Spain by that time. Variable AOU values, ranging from −5 to −20 μmol kg^{-1}, were observed both in the PCCC and in the coastal domains during the late spring cruise.

In our analysis of the chemical features of ENACW transported by the PCCC, seawater samples between the shallow ENACWst salinity maximum at 26.6–26.8 σ_0 (50–100 m depth) and the deep ENACWsp salinity minimum at 27.2 σ_0 (450–500 m depth) have been selected from the set of sampling stations in the area defined by latitudes 42° and 43°N, and longitudes 11°W (−11°E) and the 1000 m isobath. Data from the sampling stations inshore of the 1000 m isobath have been rejected owing to the effect of shelf mineralisation processes on the nutrient–temperature relationships of ENACW. A total of 395 samples have been considered.

The resulting θ/S diagram (not shown) exhibits the expected positive linear relationship between tempera-

ture and salinity ($r = +0.94$ Table 3), with ENACW temperatures ranging from 10.5 to 15 °C. The standard error of the salinity (±0.05) and temperature (±0.4 °C) estimates from the θ/S regression are of the order of magnitude of the variability observed for ENACW by Pérez et al. (1995). These authors found a decadal cycle of salinity/temperature changes of ENACW in parallel to the decadal changes of $-Q_X$ (Fig. 2(d)). Accordingly, a clear salinity excess of +0.05 and/or temperature deficit of −0.4 °C were/was observed at the time of GALICIA-XII (1991), and MORENA-I and -II (1993) compared with the GALICIA-VI and -VII (1983–1984) and the CD110b and Bg9815c (1998).

The chemical characteristics of ENACW transported by the PCCC have been studied by regression analysis of selected samples. C_T, nitrate and phosphate show a significant negative correlation with temperature throughout the ENACW domain ($r < -0.89$; Table 3). C_T has been normalised to salinity 35.0 and corrected for calcium carbonate precipitation-dissolution (NC_Tcor) by subtracting $-0.5 \times (NTA + NO_3)$, according to Broecker and Peng (1982). We find that a quadratic regression model provides a better explanation for the silicate–temperature relationship ($r = -0.94$), indicating that ENACWsp is silicate-richer than ENACWst. This maybe expected from the relatively higher silica fluxes in subpolar than in subtropical waters (Nelson, Treguer, Brzezinski, Leynaert, & Queguiner, 1995). The regression was lower in the case of the AOU of ENACW transported by the PCCC ($r = -0.82$). Álvarez-Salgado et al. (2002) have recently pointed out that the nutrient anomalies of the regressions with temperature (ΔNO_3^-, HPO_4^{2-} and ΔSiO_4H_4) are not significantly correlated with the corresponding salinity anomalies (ΔS; $r < 0.20$), suggesting that nutrient anomalies are the result of the observed decadal changes in the thermohaline properties of ENACW. Our study confirms a similar observation for the AOU and NC_Tcor anomalies (ΔAOU and ΔNC_Tcor). Assuming that temperature removes the effect of ENACW mixing, then the ΔAOU, ΔNC_Tcor, ΔNO_3^-, ΔHPO_4^{2-} and ΔSiO_4H_4 variabilities must result from differences in biogeochemical processes. Thus, carbon and nutrient anomalies were well correlated, with a C/N/P molar ratio of 108 ± 12/16.7 ± 0.6/1 (Table 3), indicating that the anomalies were the result of rapid mineralisation of sinking organic particles of Redfield composition (Anderson & Sarmiento, 1994). Silicate and nitrate anomalies were also well correlated ($r = +0.79$), with an N/Si molar ratio of 2.4 ± 0.1. Following the Redfield ratios observed in carbon and nutrient anomalies, an $\Delta AOU/\Delta NO_3^-$ ratio of 9–10 $molO_2\ molN^{-1}$ would be expected. However, despite the relatively high correlation between AOU and nitrate anomalies ($r = +0.92$), the O_2/N molar ratio was only 6.8 ± 0.2; that is about 70% of the expected Redfield value. This would seem to result from the study area being within the North Atlantic ventilated thermocline where the ENACWsp forms (Castro, Pérez, Holey, & Ríos, 1998). As a consequence, AOU levels in the cold and nutrient-rich ENACWsp

Table 3
Equations, correlation coefficients (r) and number of data points (n) used in AOU (μmol kg^{-1}), NC_T (μmol kg^{-1}), nutrient (μmol kg^{-1}) and salinity temperature (°C) regressions and their anomalies for the selected ENACW samples

Regression equation	r	n
$S(\pm 0.05) = 35.792(\pm 0.003) + 0.121(\pm 0.002) \times [\theta - 13]$	+0.94	395
$AOU(\pm 8.8) = 21.9(\pm 0.5) - 12.0(\pm 0.4) \times [\theta - 13]$	−0.82	390
$NC_Tcor(\pm 8.6) = 917(\pm 1) - 19.5(\pm 0.4) \times [\theta - 13]$	−0.92	382
$NO_3^-(\pm 1.3) = 6.1(\pm 0.1) - 3.43(\pm 0.07) \times [\theta - 13]$	−0.94	382
$HPO_4^{2-}(\pm 0.08) = 0.38(\pm 0.01) - 0.180(\pm 0.004) \times [\theta - 13]$	−0.92	375
$SiO_4H_4(\pm 0.5) = 1.89(\pm 0.04) - [1.04(\pm 0.03) - 0.26(\pm 0.02) \times (\theta - 13)] \times [\theta - 13]$	−0.94	379
$\Delta AOU(\pm 4.8) = 6.8(\pm 0.2) \times \Delta NO_3^-$	+0.84	359
$\Delta NC_Tcor(\pm 6.9) = 6.5(\pm 0.5) \times \Delta NO_3^-$	+0.57	359
$\Delta NO_3^-(\pm 0.7) = 16.7(\pm 0.6) \times \Delta HPO_4^{2-}$	+0.83	359
$\Delta NO_3^-(\pm 0.8) = 2.4(\pm 0.1) \times \Delta SiO_4H_4$	+0.79	359

branch are much lower than expected from the carbon and nutrient distributions as a result of intense ventilation of the water mass just outside the study area, where mixed layer depths may exceed 500 m.

3.3.2. Seasonal development of nitrite profiles in relation to the stratification/mixing sequence of PCCC waters

In the coastal domain, nitrite (NO_2^-) profiles at the time of the onset of the PCCC (Fig. 10(a)) were characterised by a small subsurface maximum of ~0.10 μmol kg^{-1} at the base of the nutricline (Fig. 9(a)). Nitrite was undetectable (<0.02 μmol kg^{-1}) both above and below this subsurface maximum. This structure was still observed in late autumn during the anomalous PCCC-favourable situation of the December 1983 (Fig. 10(b)). Moreover, relatively high NO_2^- levels were observed in the surface mixed layer of both the coastal (>0.2 μmol kg^{-1}) and the PCCC (0.05–0.10 μmol kg^{-1}) domains during the PCCC-unfavourable years, e.g. in November–December 1993 (Fig. 10(c)). Surface mixed layer NO_2^- levels in the PCCC domain were ~0.15 μmol kg^{-1} during the January 1998 and ~0.25 μmol kg^{-1} during the February–March 1984. The increase of NO_2^- from late autumn to late winter in the PCCC domain paralleled the progressive deepening of the winter mixed layer from 60 m (November–December 1993) to 125 m (January 1998) and to 150 m (February–March 1984). Surface mixed layer NO_3^- concentrations (Fig. 9(c), (d) and (e)) also increased in parallel with those of NO_2^-. The subsurface NO_2^- maximum reformed again during spring, in both the coastal and the PCCC domains, with high values (>0.20 μmol kg^{-1}) occurring at the nitracline (Fig. 10(f)). In contrast, an intrusion of saline water with high NO_2^- (~0.20 μmol kg^{-1}) was observed at the Cantabrian shelf break (Bay of Biscay), in April 1987 (Bode et al., 1990), resembling the structure observed off 42°–43°N during the winter. This suggests that in spring off the Bay of Biscay the PCCC retains the mixing conditions observed off the western coast during the winter. During summer (June–July 1998), the subsurface NO_2^- maximum was very weak when the poleward flow was represented only by the undercurrent (Fig. 10(g)).

A subsurface NO_2^- maximum is a common feature of N-limited oligotrophic systems, where it is usually referred to as the 'primary nitrite maximum' (PNM; Wada and Hattori, 1991). A PNM is observed in shelf waters off NW Spain during the relaxation periods between consecutive upwelling pulses throughout the upwelling-favourable season, when the system switches from meso- to oligotrophic conditions (Figueiras & Ríos, 1993). The feature is also observed in the adjacent stratified and nitrogen-exhausted oceanic waters (Castro, Pérez, Álvarez-Salgado, & Fraga, 2000), and is generally found at the 'level of no motion' between the southward flowing surface layer and the northward flowing Portugal Coastal Under Current (Batteen et al., 2000).

Enhanced light inhibition of bacterial oxidation of NO_2^- to NO_3^- compared with NH_4^+ oxidation to NO_2^- is commonly cited as the main reason for the formation of the PNM in oligotrophic waters (Dore & Karl, 1996; Olson, 1981a; Wada & Hattori, 1991). Therefore, the presence of the PNM during the autumn and spring cruises could be explained by the oligotrophic waters of subtropical origin conveyed by the PCCC to temperate/subpolar latitudes. However, the large NO_2^- excess observed in the PCCC surface mixed layer during the winter cruises when NO_3^- concentrations are relatively high (>1.5 μmol kg^{-1}) does not occur under oligotrophic conditions. Liberation of NO_2^- from phytoplankton during assimilative NO_3^- reduction has been documented (Dore & Karl, 1996; Kiefer, Olson, & Holm-Hansen, 1976; Olson, 1981b; Vaccaro & Ryther, 1960) with the amount of NO_2^- produced varying inversely with the intensity of light. This is consistent with the observed increase of NO_2^- concentration in parallel to surface mixed layer deepening through the winter. Therefore, it seems that under these low-light conditions, phytoplanktons are able to efficiently reduce NO_3^- to NO_2^- while the conversion of NO_2^- to NH_4^+ (which requires much more energy and reduction power) becomes the limiting step in the NO_3^- assimilatory pathway (Blasco, 1971). It should be noted that the phytoplankton species in the NW Iberian margin are adapted to the winter light conditions, but the maximum production per unit of Chl-*a*, $P_m^B = 1.4 \pm 0.4$ gC (gChl-*a*)$^{-1}$ h^{-1}, is less than 1/3 of the summer values (see Section 3.4.3; Table 4), which should affect their

Table 4
Average±SD photosynthetic parameters (P_m^B, α^B, E_k), depth of the photic layer ($Z_{0.1\%}$, 0.1% of incident light at the surface), integrated primary production rate (PP) and integrated Chl-*a*, in the photic layer of PCCC and in the coastal waters during the GALICIA-XII (September 1991), MORENA-I (May 1993) and CD110b (January 1998) cruises

Cruise-domain	P_m^B gC (gChl h)$^{-1}$	α^B (gC(gChl)$^{-1}$ h^{-1}) (μmol m^{-2} s^{-1})$^{-1}$	E_k μmol (m^2 s)$^{-1}$	$Z_{0.1\%}$ (m)	PP mgC (m^2 d)$^{-1}$	Chl-*a* mgChl (m^2)$^{-1}$
September 1991-PCCC	4.14 ± 2.77	0.027 ± 0.015	216 ± 199	81 ± 14	356 ± 134	28 ± 6
September 1991-coastal	7.39 ± 3.82	0.049 ± 0.025	186 ± 143	70 ± 5	2126 ± 709	32 ± 5
May 1993-PCCC	4.77 ± 2.1	0.063 ± 0.03	103 ± 77	97 ± 26	776 ± 295	36 ± 7
May 1993-coastal	4.08 ± 2.7	0.052 ± 0.03	120 ± 108	71 ± 1	393 ± 108	30 ± 11
January 1998-PCCC	1.42 ± 0.4	0.04 ± 0.02	41 ± 13	55 ± 4	138 ± 44	54 ± 6
July 1998-coastal	2.93 ± 0.8	0.02 ± 0.004	156 ± 70	70	2057	219
July 1998-ocean	4.15 ± 1.65	0.039 ± 0.014	126 ± 67	80 ± 15	506 ± 116	24 ± 5

Data for coastal (upwelled) and oceanic (stratified) waters, during the Bg9815c cruise (June–July 1998), are also presented for comparative purposes.

energy and reduction-power resources. This phytogenic hypothesis is not inconsistent with the release of NO_2^- by active bacterial regeneration (Wada & Hattori, 1991) and/or grazing by microflagellates on bacteria, which also enhance the release of NO_2^- to the water column (Rault, Sohier, Rivier, & Daumas, 1988).

3.4. New insights on the effects of the PCCC on the distributions of biological parameters

Horizontal and vertical distributions of Chl-*a* and key plankton taxa illustrate the biological consequences of the onset, development and cessation of the PCCC off NW Spain. High Chl-*a* concentrations, created primarily by large diatoms and dinoflagellates, were observed on the shelf, whereas low Chl-*a* concentrations, associated particularly with small phytoplankton species, predominated in PCCC waters, where there was a higher proportion of small flagellates during winter and small dinoflagellates, mainly *Gymnodinium* spp., during autumn (Section 3.4.1). Shelf-edge exchange of plankton species is prevented by the convergent front created by the PCCC on the slope; coastal diatoms were totally absent from the PCCC domain (Section 3.4.2). Enhanced sedimentation of coastal plankton over the shelf contributed substantially to the observed nutrient enrichment of shelf bottom waters. The lower phytoplankton biomass being carried by the PCCC exhibited lower production rates than the plankton present in the coastal waters during the autumn, whereas primary production was higher in PCCC than in shelf waters during late spring. The photosynthetic parameters and the depth of the photic layer are invoked to explain the differences observed in the productivity of PCCC and of coastal phytoplankton (Section 3.4.3).

3.4.1. Effect of the PCCC on the Chl-a distributions

Over 1000 individual SeaWiFS passes from September 1997 to January 2001 have been analysed to produce synoptic chlorophyll and ocean colour fields for the western Iberian Peninsula. In order to describe the ocean colour characteristics of the PCCC and surrounding shelf and oceanic waters, a sequence of four clear images from October 1997 and January, February and March 1998 was selected for two reasons: first, the only cruise described herein to sample the PCCC subsequent to the launch of SeaWiFS took place in January 1998; secondly, the PCCC in winter of 1997/1998 exhibited a distinct signal in the SST data.

The SeaWiFS data are presented in Fig. 11, along with the corresponding SST data. Fig. 11(a) illustrates the SST of 29 October 1997. A distinct warm band, the PCCC, can be seen extending off the western coast, which turns right off Cape Finisterre to enter the Cantabrian Sea. As a consequence of the convergence created by the warm band, high levels of Chl-*a* have accumulated along the coast, which contrasts with the oligotrophic conditions prevailing in the PCCC and surrounding oceanic waters (Fig. 11(b)). On 21 January 1998 (at the end of the CD110b cruise) the warm band had extended into the Cantabrian sea and an anticyclonic eddy had formed north of Cape Ortegal (Fig. 11(c)). This feature is similar in location to a slope water oceanic eddy (SWODDY) visible in satellite data presented by Pingree and Le Cann (1990). The chlorophyll image (Fig. 11(d)) shows there were high concentrations over the shelf associated with a cooler band of water, which formed a distinct front along the 200 m contour and extended out as far as the 2000 m isobath at 42.4°–43°N. However, the colour composite (Fig. 11(e)) shows that the chlorophyll retrieval on the shelf is affected by high scattering probably because of suspended particulate matter associated with river-runoff and absorption by coloured dissolved organic matter: Fig. 12(d) shows an in situ chlorophyll value of 0.85 mg m^{-3} from CD110b data, compared to ~2.2 mg m^{-3} SeaWIFS estimate at the same location, albeit 6 d later. Hence, care must be taken interpreting winter estimates of chlorophyll on the shelf. The PCCC, in contrast with the SST, does not exhibit a distinct signal in the ocean colour data south of 42°N. Pelíz and Fiúza, (1999) noted that the PCCC stand out from shelf or oceanic waters if it possessed a distinct colour signature, related to different levels of chlorophyll: during winter the chlorophyll field is relatively uniform off-shelf with higher concentrations on the shelf.

One month later, on 24 February 1998, the PCCC and SST signatures (Fig. 11(f)) were similar in appearance to the January image and SeaWiFS (Fig. 11(g)) again shows elevated chlorophyll concentrations on the shelf. In contrast to January, the colour composite (not shown) exhibits absorption as opposed to scattering suggesting that the enhanced chlorophyll is associated with phytoplankton growth. There was a sharp front aligned with the coast extending over the 200 m contour and coincident with cooler coastal water. The chlorophyll concentration dropped sharply across this front from ~1.7 to 0.45 mg m^{-3} at 43°N. Chlorophyll concentration within the PCCC appeared slightly higher than waters further offshore. The SST image appeared to show a second warm 'PCCC-like' band extending northward between 12°–13°W and 40°–41°N.

Fig. 11(h) and (i) illustrates the SST and chlorophyll data for 24 March 1998. The warmer SSTs associated with the PCCC were no longer pronounced north of 43°N and at 43.5°N 9.2°W SST had progressively decreased from 15.5 °C in January, to 14.7 °C in February and further to 14.1 °C in March. There were elevated chlorophyll concentrations in a narrow band along the coast, and offshore of 11°W between 41° and 43°N that may have been the first indication of the onset of the spring bloom. Between the shelf and offshore waters there was a wedge of low chlorophyll water that was associated with the warmer SST of the PCCC. This feature was observed by Pelíz and Fiúza (1999) on individual CZCS images in spring (typically in May) and on monthly composite images for May and October–November. The appearance in March 1998 was explained by Joint et al. (2002) who analysed SeaWiFS images for the region, who suggested that the Spring bloom occurred earlier in 1998 than 1999; a similar early occurrence was observed again in March 2000. The low chlorophyll wedge was visible on SeaWiFS monthly composites including March and October 1998 and May and October 1999 (see Fig. 11(j) and (k)).

In addition to the synoptic overview provided by the selected SeaWIFS images, Chl-*a* was measured during the cruises. Surface Chl-*a* distributions (Fig. 12) show that the main consequence of the low chlorophyll PCCC in the NW Iberian margin was its ability to restrict coastal plankton to the shelf region. The influence was marked during early autumn (September 1991, Fig. 12(a)), late autumn (November–December 1993, Fig. 12(c)) and late winter (February–March 1984, Fig. 12(e)), but less so in mid-winter (January 1998, Fig. 12(d)) and late spring (May 1993, Fig. 12(f)) because Chl-*a* concentrations were higher in the coastal waters during the former than the latter cruises. Although retention of the coastal 'autumn bloom' on the shelf at the time of the onset of the PCCC in September 1986 has been previously described by

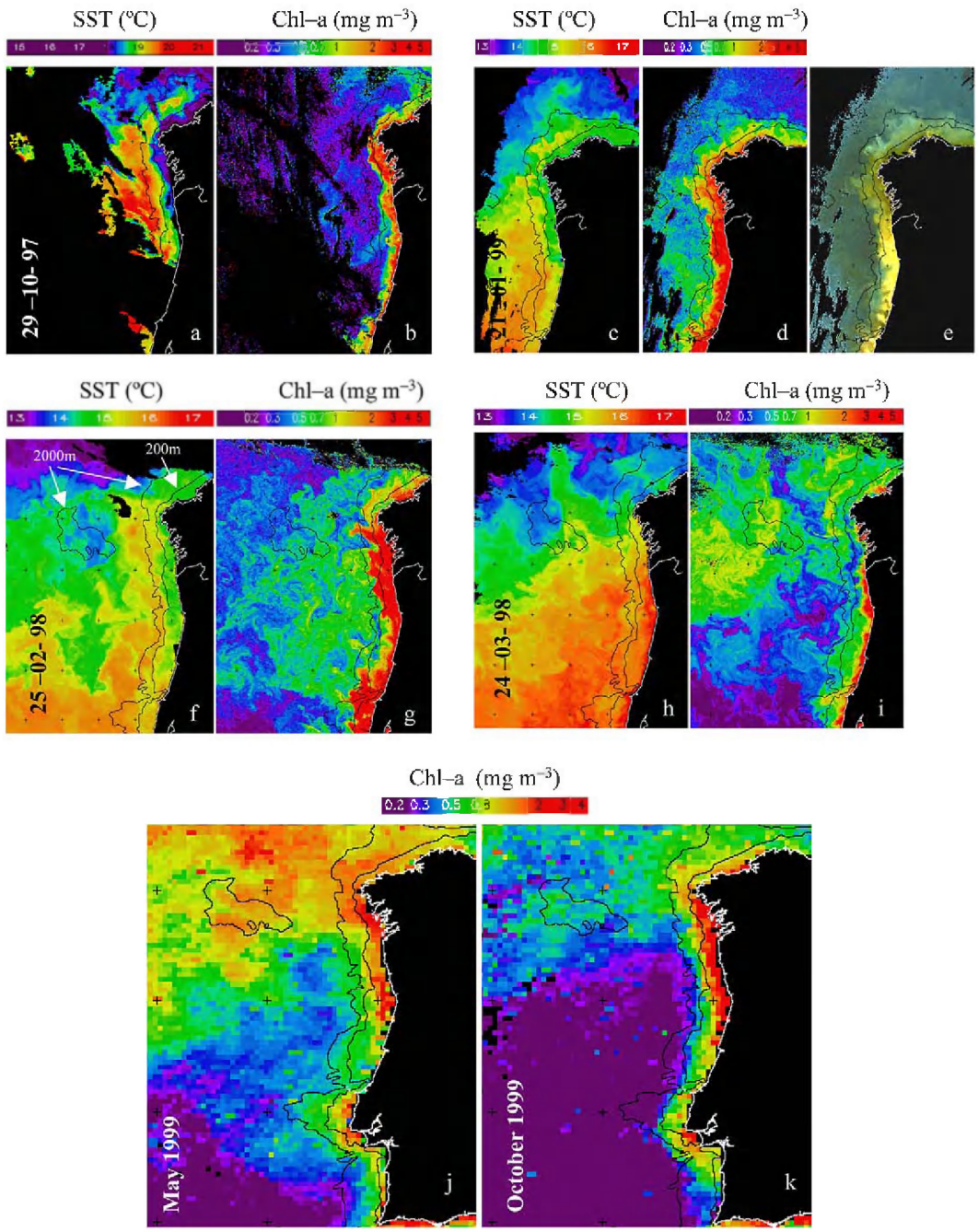

Fig. 11. Satellite images from: 29 October 1997, AVHRR-SST (a); SeaWiFS Chl-*a* (b); 21 January 1998, AVHRR-SST (c); SeaWiFS Chl-*a* (d); SeaWiFS colour composite of 555, 510 and 443 nm bands (e); 25 February 1998, AVHRR-SST (f); SeaWiFS Chl-*a* (g); 24 March 1998, AVHRR-SST (h); SeaWiFS Chl-*a* (i). SeaWiFS monthly composites for May 1999 (j), and October 1999 (k). Note different Chl-*a* scales for image (h) and (i). The 200 and 2000 m depth contours are marked on each image. AVHRR-SST in °C and SeaWiFS Chl-*a* in mg m^{-3}.

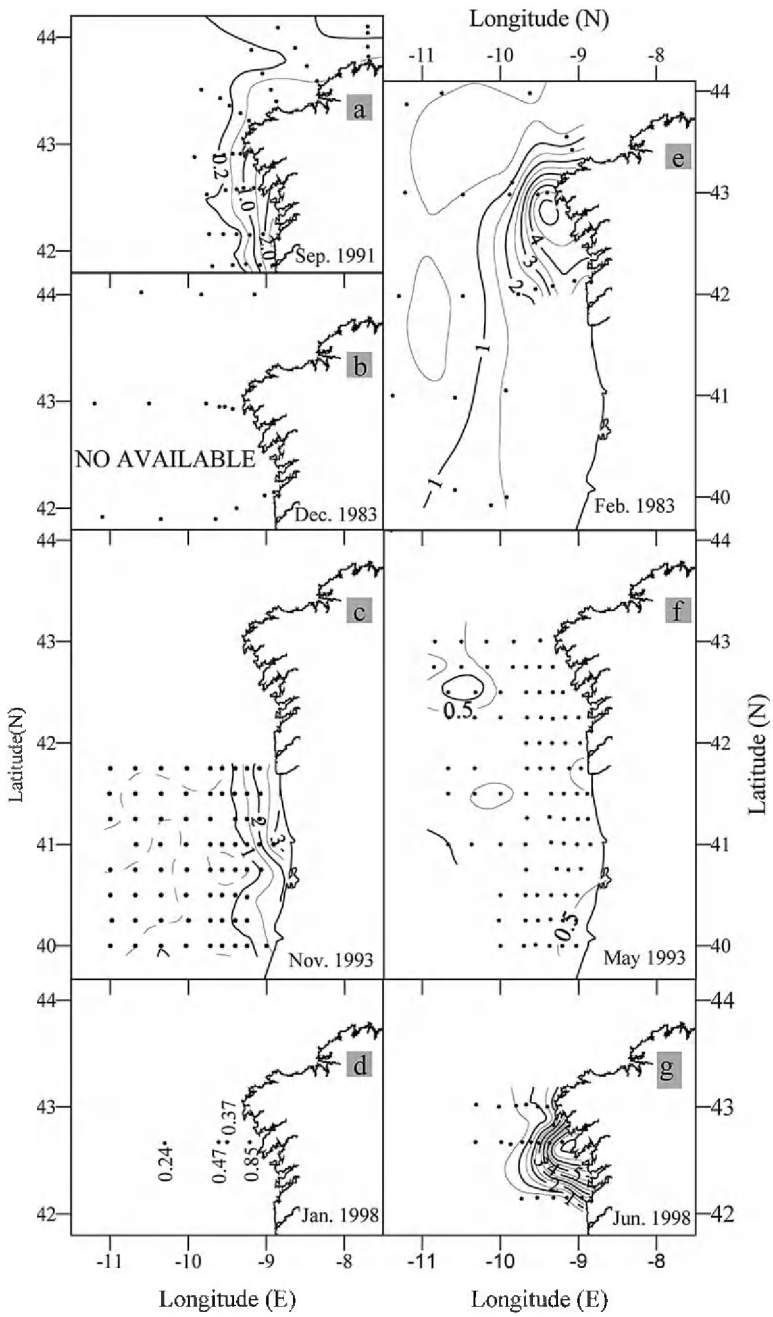

Fig. 12. Horizontal distributions of surface Chl-*a* (μg l^{-1}) during the GALICIA-XII (September 1991) (a), GALICIA-VI (November–December 1983) (b), MORENA-II (November 1993) (c), CD110b (January 1998) (d), GALICIA-VII (February–March 1984) (e), MORENA-I (May 1993) (f), and Bg9815c (July 1998) (g) cruises.

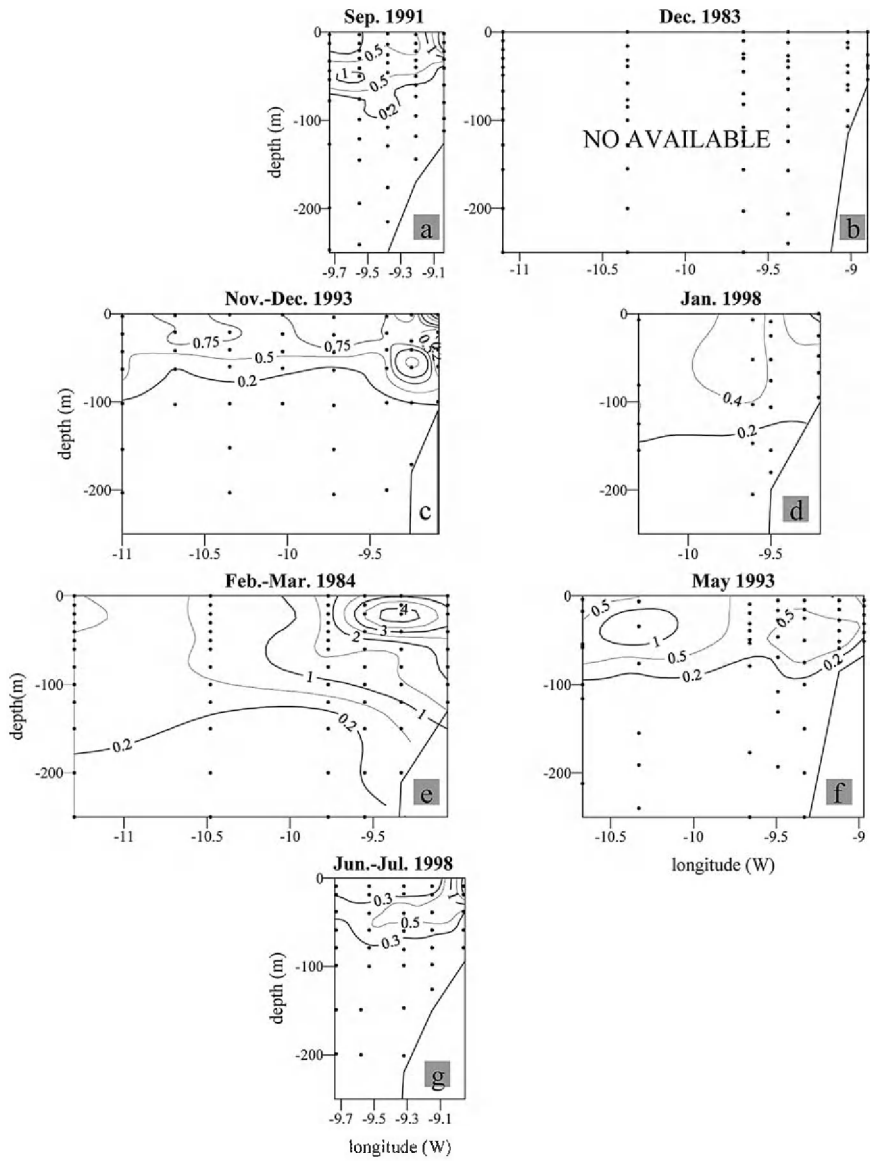

Fig. 13. Vertical distributions of chlorophyll-a (mg m^{-3}) along the zonal lines indicated in Fig. 1 during the GALICIA-XII (September 1991) (a), GALICIA-VI (November–December 1983) (b), MORENA-II (November 1993) (c), CD110b (January 1998) (d), GALICIA-VII (February–March 1984) (e), MORENA-I (May 1993) (f), and Bg9815c (July 1998) (g) cruises.

Castro et al. (1997), the corresponding confinement of the coastal spring bloom is described here for the first time (Fig. 12(e)). The convergent front created by the PCCC favours the sedimentation and benthic mineralisation of the spring bloom materials formed in the shelf waters of the NW Iberian margin rather than its off-shelf export. Contrary to what may be expected for an upwelling system, the co-ocurrence of the spring bloom and the PCCC would produce intense recycling of the new primary production in the coastal domain. The Chl-*a* distribution in February–March 1984 presents a good example of the difference between 'new' and 'export' production. This observation has important implications in relation to the

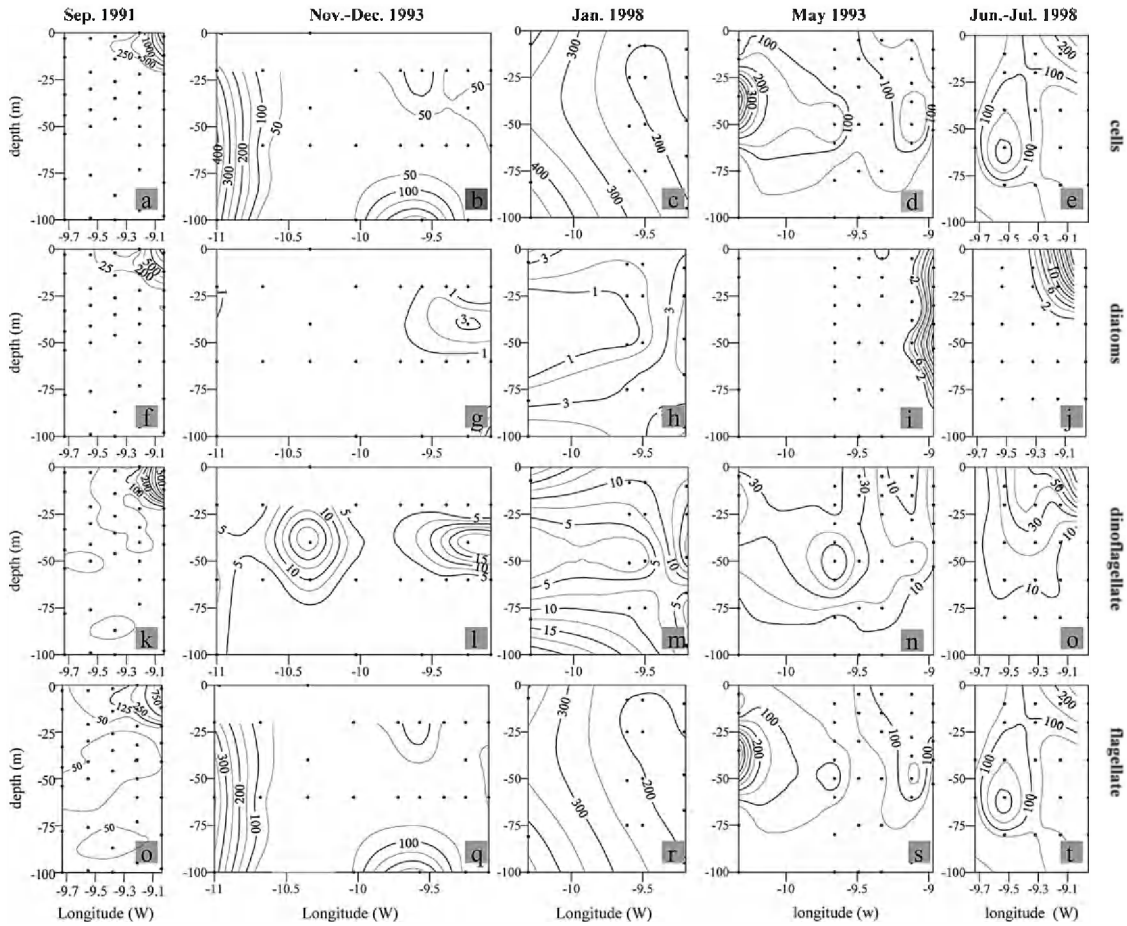

Fig. 14. Vertical distributions along the zonal lines indicated in Fig. 1 of plankton numbers (cell ml^{-1}) during the GALICIA-XII (September 1991) (a), MORENA-II (November 1993) (b), CD110b (January 1998) (c), MORENA-I (May 1993) (d), and Bg9815c (July 1998) (e) cruises; diatom numbers (cell ml^{-1}) during the September 1991 (f), November 1993 (g), January 1998 (h), May 1993 (i), and July 1998 (j) cruises; dinoflagellate numbers (cell ml^{-1}) during the September 1991 (k), November 1993 (l), January 1998 (m), May 1993 (n), and July 1998 (o) cruises; and flagellate numbers (cell ml^{-1}) during the September 1991 (p), November 1993 (q), January 1998 (r), May 1993 (s), and July 1998 (t) cruises.

potential capacity of coastal upwelling systems to absorb atmospheric CO_2. If the new production of the spring bloom is recycled rather than exported, then, the net effect of the biological CO_2 pump is nil. Although, to our knowledge, similar conditions have not been described for other coastal upwelling systems, it would seem likely that they may occur in hydrographically comparable areas.

Low surface Chl-*a* concentrations on the shelf during the early winter and late spring cruises (Fig. 12(d) and (f)) were caused by the strong mixing conditions encountered during the winter (Fig. 7(d)), which reduce phytoplankton concentrations in the mixed layer, and by the low surface nutrient concentrations during late spring (Figs. 8(f) and 9(f)), which limit phytoplankton growth. In contrast, during the upwelling season (Fig. 12(g)), high chlorophyll values (>7 mg m^{-3}) were recorded off the Rías Baixas and the surface distributions suggest there was off-shelf export of this fresh material.

The vertical distributions of Chl-*a* (Fig. 13) confirm that the highest concentrations were located over the shelf, and also reveal that a subsurface chlorophyll maximum was located at ~50 m, and persisted from

the cessation in late spring (May 1993) to the onset in early autumn (September 1991) of the PCCC. The subsurface chlorophyll maximum, which extended from the shelf break to the open ocean waters, coincided with the presence of stratified oceanic surface waters (Fig. 7) and low mixed layer nutrient concentrations (NO_3^- <0.5 μmol kg^{-1}; Fig. 9) in the area. In contrast, the stronger vertical mixing conditions during the period of maximum PCCC development (January 1998; Fig. 13(d)) determined the quasi-homogenous distribution of Chl-*a* over the surface 100–150 m. High Chl-*a* concentrations in shelf surface waters and a subsurface maximum in the adjacent stratified ocean waters are typical of coastal upwelling systems (e.g. Basterretxea & Arístegui, 2000). Chl-*a* concentrations in the subsurface maximum (>0.5 mg m^{-3}, Fig. 12(a) and (g)) were similar to values recorded in other mesotrophic areas, such as the Kuroshio Current off Japan (Takahashi, Nakai, Ishimaru, Hasumoto, & Fujita, 1985), the western Mediterranean (Estrada, 1985) and the off-shelf waters of the NW African upwelling system (Basterretxea & Arístegui, 2000). We also note that the relatively high Chl-*a* concentrations in the deep upper mixed layer (>100 m) of the PCCC domain during the winter produced integrated water column Chl-*a* concentrations greater than those observed during the spring, summer and autumn (Table 4).

3.4.2. Isolation of PCCC from coastal plankton species

The action of the PCCC in restricting the cross shelf-edge exchange of materials also has a marked effect on the distribution of phytoplankton abundances in the study area during the onset (September 1991) of the PCCC, when the autumn bloom exported from the Rías Baixas (diatom numbers >2000 cell ml^{-1}; Fig. 14(f)), was confined in the shelf. Accumulation of dinoflagellates (Fig. 14(k)) and flagellates (Fig. 14(p)) on the shelf was also observed during this cruise. When southerly winds strengthen but rainfall remains low (high Q_X/R ratio), meteorological conditions that can occur at the beginning of the autumn, the PCCC can favour dinoflagellate blooms, sometimes of toxic species, inside the Rias Baixas. It has been argued that these blooms may develop either through selection of species already present in the interior of the Rias Baixas (e.g. Figueiras et al., 1994) or following the entrainment of oceanic phytoplankton assemblages (e.g. Fraga, Bravo, & Reguera, 1993).

The late autumn (November–December 1993) and winter (January 1998) cruises showed vertically homogeneous phytoplankton distributions, with a strong dominance of small flagellates (Fig. 14(b), (c), (q) and (r)), but an almost complete absence of diatoms (Fig. 14(g) and (h)) and dinoflagellates (Fig. 14(l) and (m)). Unfortunately, no samples were available from the surface waters of the coastal stations during the November–December 1993 cruise, where a Chl-*a* maximum of 3 mg m^{-3} was found (Fig. 13(c)). Small flagellates were more abundant at the westernmost oceanic stations during both cruises, confirming that in winter PCCC waters are associated with mainly this phytoplankton grouping. Small flagellates were also dominant in PCCC waters during the May 1993 cruise (Fig. 14(d) and (s)) while dinoflagellates (small *Gymnodinium* spp.) were also relatively important (Fig. 14(n)). The most striking feature of the late spring PCCC event, as deduced from the vertical distributions, was the confinement of diatoms to the narrow band of coastal waters (Fig. 14(i)). Sedimentation of the diatoms is favoured at the convergence adjacent to the slope.

Diatoms were also confined in coastal waters during upwelling in June–July 1998 (Fig. 14(j)), whereas dinoflagellates were exported further offshore (Fig. 14(o)) in the surface layer. In contrast, the subsurface Chl-*a* maximum at 50 m (Fig. 14(e)) was constituted primarily by small flagellates (Fig. 14(t)). The swimming capacity of dinoflagellates allows them to remain in the surface layer during off-shelf export, whereas diatoms sediment out of the stratified waters. Diatoms are able to remain in the surface layer only in well-mixed water columns as they occur during upwelling. During a recent Lagrangian study of the off-shelf export of materials produced in the upwelling centre of Cape Finisterre, mediated through the Rías Baixas filament described by Haynes et al. (1993), Joint et al. (2001) recorded a similar situation with the diatoms being confined on the shelf but the dinoflagellates being exported by the filament.

3.4.3. Primary production rates in PCCC and coastal waters

Primary production (PP; Table 4) in coastal waters confined by the PCCC was higher during early autumn (September 1991; 2.1 ± 0.71 gC m^{-2} d^{-1}) than during late spring (May 1993; 0.4 ± 0.11 gC m^{-2} d^{-1}) despite the fact that integrated Chl-*a* levels and photic layer depths were similar during the two cruises (Table 4). The day length was longer in the less-productive spring period (15 h) than during the autumn cruise (11 h), indicating that the difference was caused by the higher maximum photosynthetic rate (P_m^B) of phytoplankton populations advected from Rías Baixas during the September 1991. In contrast, PP rates in the PCCC domain were higher during late spring (0.78 ± 0.3 gC m^{-2} d^{-1}) than in the autumn (0.4 ± 0.13 gC m^{-2} d^{-1}). Since the comparable values of P_m^B were similar in this instance ($p = 0.55$), the higher PP in late spring is likely to be the result of the longer day length and the slightly deeper photic layer at this time. Photosynthetic efficiency (α^B) of the phytoplankton in the PCCC waters during the May 1993 cruise was higher than in September 1991 ($p < 0.01$) and, consequently, the light saturation parameter E_k was lower in the late spring in May 1993. This indicates that photosynthesis was light saturated at lower irradiances in late spring than in autumn and, this may partially explain the higher PP in spring.

PP in PCCC waters was low during the winter (January 1998; 0.14 ± 0.044 gC m^{-2} d^{-1}) despite the phytoplankton populations being low-light adapted (E_k = 41 ± 13 µmol m^{-2} s^{-1}) and the integrated Chl-*a* being higher than during autumn and late spring PCCC events (Table 4). The reason for the low winter PP appears to be the extremely low P_m^B = 1.4 ± 0.4 gC (gChl - a)$^{-1}$ h^{-1}. The low-light adaptation of photosynthesis in the PCCC waters in winter reflects the strong mixing of the water column (~125 m), which was deeper than the photic layer, implying that the average light received by the phytoplankton was low. In addition, as indicated in Section 3.3.2, insufficient P_m^B rates were available to meet the energy and reduction-power requirements to efficiently reduce NO_2^- to NH_4^+, inducing the accumulation of NO_2^- in the upper mixed layer (Fig. 10(d)).

Recently upwelled coastal waters in summer (June–July 1998, Table 4) showed PP not substantially different from those of confined coastal waters in autumn (September 1991). Low maximum photosynthetic rates (P_m^B) contributed significantly to the low PP since integrated Chl-*a* concentrations were significantly higher in summer than in autumn. However, PP in the oceanic stratified waters in summer was between the autumn and late spring values. It would seem likely that the lower E_k of the oceanic waters compared to the PCCC waters accounted for the higher PP in summer, since integrated Chl-*a* in the photic layer and P_m^B at this time were similar. The lower E_k values indicate that photosynthesis was light saturated at lower irradiance values during summer than in autumn. In late spring PP was higher in PCCC waters than in summer stratified waters as a result of the higher integrated Chl-*a* concentrations in the photic layer; here P_m^B and E_k values were not significantly different between cruises ($0.51 < p < 0.53$).

PP values reported in the present study compare favourably with the monthly average satellite-derived production rates of the PCCC domain in this area presented by Joint et al. (2002). It should be noted that these authors have used part of the PP data used in this paper (those of the June–July 1998 and January 1998 cruises) to produce their satellite-derived estimates. Teira, Serret, and Fernández (2001) have reported PP rates for the October 1998 PCCC conditions. Their average value of 491 ± 65 mgC m^{-2} d^{-1} compares very well with our value of 356 ± 134C mgC m^{-2} d^{-1} during September 1991 (Table 4). Values in the coastal domain during June–July 1998 (2.1 gC m^{-2} d^{-1}, Table 4) should be considered as the lower limit of possible PP rates during the upwelling season. Values ranging from 3.2 to 7.4 gC m^{-2} d^{-1} have been reported by Teira et al. (2001) and, exceptionally, as much as 10 gC m^{-2} d^{-1} has been measured in shelf waters off the Rías Baixas during the spring bloom by F.G. Figueiras (personal communication). Discarding extremely high spring bloom and extremely low winter values (0.14 gC m^{-2} d^{-1}; Table 4), the range of PP rates off NW Spain was similar to those recorded in the Benguela (0.5–4 gC m^{-2} d^{-1}; Brown & Field, 1986; Brown, Painting, & Cochraine, 1991; Estrada & Marrasé, 1987), the Peru (1.9 gC m^{-2} d^{-1}; Barber & Smith, 1981) and the California (0.5–2.6 gC m^{-2} d^{-1}; Pilskan, Paduan, Chavez, Anderson, & Berelson, 1996) coastal upwelling systems.

4. Summary and major conclusions

Combination of available wind-stress data, satellite-derived SST and chlorophyll distributions and hydrographic data collected during seven cruises off the NW Iberian margin together with comparable published information have allowed us to study the effects of the PCCC on the chemistry and biology of the NW Iberian margin during the previously little studied downwelling-favourable season (September–May), when the PCCC develops. In summary the novel contributions of this paper to the knowledge of the PCCC are:

1. On the modes of variability of the coastal winds off NW Spain: alongshore coastal wind-stress, a major modulating agent of the direction and intensity of the coastal circulation, exhibits a remarkable short time-scale variability, with 66% (average 1982–1998) being concentrated in periods ≤30 d. The seasonal cycle of upwelling-favourable winds, from the beginning of April to the end of September, and downwelling-favourable winds, the rest of the year, only explains from <5 to >27% of the coastal wind variability (1982–1998 average, 12%). The onset of the downwelling-favourable season is temporally restricted between mid-September and mid-October—the time of the autumn plankton bloom. Its termination can occur any time from early February to late May, and may or may not coincide with the spring plankton bloom. Marked interannual variability was observed from 1982 to 1998, with a long-term cycle of ~10 year period, associated with the basin-scale NAO, clearly defining PCCC favourable and unfavourable years.
2. On the stratification/homogenisation cycle in PCCC waters: the warm and salty surface and central waters being transported by the PCCC undergo a marked seasonal cycle of stratification and vertical overturn, with the upper mixed layer depths gradually increasing from 20 m in late summer–early autumn, to 60 m in late autumn, to 125 m in early winter and finally to 150 m in late winter. This cycle has important implications for the chemistry and biology of PCCC waters.
3. On the seasonal evolution of nitrite profiles in PCCC waters: the seasonal progression of nitrite concentrations in PCCC waters undergoes a remarkable cycle related to the stratification/homogenisation cycle of the upper water column. A brief subsurface maximum <0.1 μmol kg^{-1} occurs during the early autumn, which evolves into a marked winter mixed layer maximum concentrations of >0.2 μmol kg^{-1}. This in turn develops to a subsurface maximum of >0.2 μmol kg^{-1} during the spring. We favour (see point 6) a 'phytogenic' rather than a 'bacteriogenic' hypothesis for this development of a nitrite maximum during the winter.
4. On the stoichiometry of mineralisation in ENACW being transported by the PCCC: ENACW transported by the PCCC is enriched with nutrients which are the products of intense mineralisation processes during poleward displacement. The resulting O_2:C:N:P mineralisation ratios are not significantly different from the Redfield values characteristic of the early degradation of the products of phytoplankton photosynthesis.
5. On the separation of PCCC and coastal plankton populations under downwelling conditions: the downwelling front on the shelf created by the PCCC separates two contrasting environments. In the coastal domain conditions are mesotrophic that are a result of the nutrient-rich waters being discharged from the Rías Baixas and accumulating on the shelf during the winter, and the intensity of remineralisation processes at the sediment–water interface during the spring and autumn. In contrast, oligotrophic conditions (<0.1 μmol kg^{-1} NO_3^-) are observed in the stratified, <20 m deep, spring and autumn surface mixed layer of the PCCC, whereas higher nutrient levels (>1.0 μmol kg^{-1} NO_3^-) occur in the >100 m deep winter mixed layer. The downwelling front is usually located at the slope, except when either strong winds blow from the south and/or continental runoff are limited, at which times the PCCC invades the shelf and may even enter the rías. The phytoplankton assemblages of PCCC waters are dominated by small flagellates, and are clearly differentiated from assemblages of the coastal waters that are dominated by larger forms (diatoms and dinoflagellates). The PCCC restricts the coastal phyto-

plankton to the shelf; an effect that is especially important at the times of the spring and autumn blooms. In this sense, the seasonal cycle of surface Chl-*a* reveals that in the Ría de Vigo maximum concentrations (>7 mg m^{-3}) occur during May and September (Nogueira et al., 1997), respectively, coincident with the onset and cessation of the PCCC. Therefore, at these particular times of the year intense PCCC events will favour the in situ mineralisation of sinking organic matter, mainly diatoms, produced at high rates in the rías-shelf system.

6. The photosynthesis response of PCCC and coastal plankton populations to downwelling conditions: primary production of coastal waters during the downwelling-favourable season depends on the seasonal evolution of the maximum photosynthetic rate ($P_m{}^B$), which is highest during autumn. Photic layer depth and day length are the two factors, which determine that primary production in PCCC waters is higher during spring than in autumn. Although Chl-*a* concentrations are higher in winter than during autumn and spring, primary production rates in PCCC waters are extremely low during the winter because of the low $P_m{}^B$ values. These low $P_m{}^B$ could be responsible for the large NO_2^- accumulation in the winter mixed layer, because the energy and reduction power obtained during phytoplankton photosynthesis may not be enough to satisfy the requirements for carbon fixation and reduction of NO_2^- to NH_4^+.

Acknowledgements

The authors wish to thank the Captain, crew and technicians of Research Vessels '*García del Cid*' (GALICIA-VI and -VII), '*Investigador S.*' (GALICIA-XII), '*Cornide de Saavedra*' (MORENA-I), '*Hakon Mosby*' (MORENA-II), '*Charles Darwin*' (CD110b) and '*Belgica*' (Bg9815c) for their help during the sampling programme. J.M. Cabanas (IEO, Vigo) has provided the Ekman transport data. T. Rellán helped with the preparation of figures. These cruises were performed with the financial support of the CICYT grant No. MAR97-2068-CE and the EU contract numbers MAS1-CT90-0017 (The Control of Phytoplankton Dominance) MAS2-CT93-0065 (MORENA) and MAS3-CT97-0076 (OMEX II-II).

References

Álvarez-Salgado, X. A., Beloso, S., Joint, I., Nogueira, E., Chou, L., Pérez, F. F., Groom, S., Cabanas, J. M., Rees, A., & Elskens, M. (2002). New production of the NW Iberian shelf during the upwelling season. *Deep-Sea Research I, 49*, 1725–1739.

Álvarez-Salgado, X. A., Castro, C. G., Pérez, F. F., & Fraga, F. (1997). Nutrient mineralization patterns in shelf waters of the Western Iberian upwelling. *Continental Shelf Research, 17*, 1247–1270.

Álvarez-Salgado, X. A., Gago, J., Miguez, B. M., Gilcoto, M., & Pérez, F. F. (2000). Surface waters of the NW Iberian upwelling system: upwelling on the shelf versus outwelling of upwelled waters from the Rías Baixas. *Estuarine Coastal and Shelf Science, 51*, 821–837.

Álvarez-Salgado, X. A., Fraga, F., & Pérez, F. F. (1992). Determination of nutrient salts by automatic methods both in seawater and brackish water: the phosphate blank. *Marine Chemistry, 39*, 311–319.

Álvarez-Salgado, X. A., Rosón, G., Pérez, F. F., & Pazos, Y. (1993). Hydrographic variability off the Rías Baixas (NW Spain) during the upwelling season. *Journal of Geophysical Research, 98*, 14447–14455.

Ambar, I., & Fiúza, A. F. G. (1994). Some features of the Portugal current system: a poleward slope undercurrent, an upwelling-related summer southward flow and an autumn–winter poleward coastal surface current. In K. B. Katsaros, A. F. G. Fiúza, & I. Ambar (Eds.), *Proceedings of the second international conference on air–sea interaction and on meteorology and oceanography of the coastal zone* (pp. 286–287). Boston, USA: American Meteorological Society.

Ambar, I., Fiúza, A. F. G., Boyd, T., & Frouin, R. (1986). Observations of a warm oceanic current flowing northward along the coasts of Portugal and Spain during November–December 1983. *EOS Transactions, American Geophysical Union, 67*, 1054.

Anderson, L. A. (1995). On the hydrogen and oxygen content of marine phytoplankton. *Deep-Sea Research I, 42*, 1675–1680.

Anderson, L. A., & Sarmiento, J. L. (1994). Redfield ratios of remineralization determined by nutrient data analysis. *Global Biogeochemical Cycles, 8*, 65–80.

Arhan, M., Colin de Verdière, A., & Memery, L. (1994). The eastern boundary of the subtropical North Atlantic. *Journal of Physical Oceanography, 24*, 1295–1316.

Bakun, A. (1973). Coastal upwelling indices, west coast of North America, 1946–71. *NOAA Technical report NMFS-671* (103 pp).

Bakun, A., & Nelson, C. S. (1991). The seasonal cycle of wind-stress curl in subtropical eastern boundary current regions. *Journal of Physical Oceanography, 21*, 1815–1834.

Barber, R. T., & Smith, R. L. (1981). Coastal upwelling ecosystems. In A. R. Longhurst (Ed.), *Analysis of marine ecosystems* (pp. 31–68). New York: Academic press.

Barton, E. D., Arístegui, J., Tett, P., Cantón, M., García-Braun, J., Hernández-Leon, S., Nykjaer, L., Almeida, C., Almunia, J., Ballesteros, S., Basterretxea, G., Escánez, J., García-Weill, L., Hernández-Guerra, A., López-Laatzen, F., Molina, R., Montero, M. F., Navarro-Pérez, E., Rodríguez, J. M., van Lenning, K., Vélez, H., & Wild, K. (1998). The transition zone of the Canary current upwelling region. *Progress in Oceanography, 41*, 455–504.

Basterretxea, G., & Arístegui, J. (2000). Mesoscale variability in phytoplankton biomass distribution and photosynthetic parameters in the Canary—NW African coastal transition zone. *Marine Ecology Progress Series, 197*, 27–40.

Batteen, M. L., Martinez, J. R., Bryan, D. W., & Buch, E. J. (2000). A modeling study of the coastal eastern boundary current system off Iberia and Morocco. *Journal of Geophysical Research, 105*, 14137–14195.

Blanton, J. O., Tenore, K. R., Castillejo, F. F., Atkinson, L. P., Schwing, F. B., & Lavín, A. (1987). The relationship of upwelling to mussel production in the rías on the western coast of Spain. *Journal of Marine Research, 45*, 497–511.

Blasco, D. (1971). Acumulación de nitritos en determinados niveles marinos por acción del fitoplancton. *Doctoral thesis*, University of Barcelona (223 pp).

Bode, A., Fernández, E., Botas, A., & Anadón, R. (1990). Distribution and composition of suspended particulate matter related to shelf-break saline intrusion in the Cantabrian Sea (Bay of Biscay). *Oceanologica Acta, 13*, 219–228.

Bordes, P., Brunel, P., & Marsouin, A. (1992). Automatic adjustment of AVHRR navigation. *Journal of Atmospheric and Oceanic Technology, 9*, 15–27.

Borges, A. V., & Frankignoulle, M. (2002). Distribution of surface carbon dioxide and air-sea exchange in the upwelling system off the Galician Coast. *Global Biogeochemical Cycles, 14*, 4-1, 4–14.

Brink, K. H., & Cowles, T. J. (1991). The coastal transition zone program. *Journal of Geophysical Research, 96*, 14367–14648.

Broecker, W. S., & Peng, T. -H. (1982). In *Tracers in the sea* (p. 690). New York: Eldigio Press.

Brown, P. C., & Field, J. G. (1986). Factors limiting phytoplankton production in a nearshore upwelling area. *Journal of Plankton Research, 8*, 55–68.

Brown, P. C., Painting, S. J., & Cochraine, K. L. (1991). Estimates of phytoplankton and bacterial biomass and production in the northern and southern Benguela ecosystems. *South African Journal of Marine Science, 11*, 537–564.

Castro, C. G., Álvarez-Salgado, X. A., Figueiras, F. G., Pérez, F. F., & Fraga, F. (1997). Transient hydrographic and chemical conditions affecting microplankton populations in the coastal transition zone of the Iberian upwelling system (NW Spain) in September 1986. *Journal of Marine Research, 55*, 321–352.

Castro, C. G., Pérez, F. F., Álvarez-Salgado, X. A., & Fraga, F. (2000). Coupling between thermohaline and chemical fields during two contrasting upwelling events off the NW Iberian Peninsula. *Continental Shelf Research, 20*, 189–210.

Castro, C. G., Pérez, F. F., Holey, S. E., & Ríos, A. F. (1998). Chemical characterisation and modelling of water masses in the North East Atlantic. *Progress in Oceanography, 41*, 249–279.

Church, J. A., Cresswell, G. R., & Godfrey, J. S. (1989). The leewin current. In S. J. Neshyba, Ch. N. K. Moores, R. L. Smith, & R. T. Barber (Eds.), (pp. 230–252). *Poleward flows along ocean eastern boundaries, coastal and estuarine studies*, Vol. 34. Berlin: Spinger.

Cresswell, G. R., & Golding, T. J. (1980). Observation of a south flowing current in the Southeastern Indian Ocean. *Deep-Sea Research, 27*, 449–466.

Dickson, A. G. (1993). pH Buffers for sea water media based on the total hydrogen ion concentration scale. *Deep-Sea Research I, 40*, 107–118.

Dore, J. E., & Karl, D. M. (1996). Nitrite distributions and dynamics at Station ALOHA. *Deep-Sea Research II, 43*, 385–402.

Estrada, M. (1985). Deep phytoplankton and chlorophyll maxima in the Western Mediterranean. In M. Moraitou-Apostolopulou, & V. Kiortsis (Eds.), *Mediterranean marine ecosystems* (pp. 247–277). New York: Plenum Press.

Estrada, M., & Marrasé, C. (1987). Phytoplankton biomass and productivity off the Namibian coast. In A. I. L. Payne, J. A. Gulland, & K. H. Brink (Eds.), *The Benguela and comparable ecosystems* (pp. 347–356). *South African Journal Marine Science*, 5.

Fedorov, K. N., & Ostrovskii, A. G. (1986). *Climatic significant physical parameters of the ocean. IOC time series of ocean measurements, vol. 3. IOC Technical series 31*. Paris: UNESCO.

Figueiras, F. G., Jones, K., Mosquera, A. M., Álvarez-Salgado, X. A., Edwards, A., & MacDougall, N. (1994). Red tide assemblage formation in an estuarine upwelling ecosystem: Ría de Vigo. *Journal of Plankton Research, 16*, 857–878.

Figueiras, F. G., & Niell, F. X. (1987). Composición del fitoplancton en la ría de Pontevedra (NO de España). *Investigación Pesquera, 51*, 371–409.

Figueiras, F. G., & Ríos, A. F. (1993). Phytoplankton succession, red tides and hydrographic regime in the Rías Bajas of Galicia. In T. J. Smayda, & Y. Shimizu (Eds.), *Toxic marine phytoplankton* (pp. 239–244). New York: Elsevier.

Fiúza, A. F. G. (1984). Hidrologia e dinâmica das aguas costeiras de Portugal. *PhD thesis*, University of Lisbon (294 pp).

Fiúza, A. F. G., Hamann, M., Ambar, I., Diaz del Río, G., González, N., & Cabanas, J. M. (1998). Water masses and their circulation off western Iberia during May 1993. *Deep-Sea Research I, 45*, 1127–1160.

Fraga, S., Bravo, I., & Reguera, B. (1993). Poleward surface current at the shelf break and blooms of *Gymnodinium catenatum* in Ria de Vigo (NW Spain). In T. J. Smayda, & Y. Shimizu (Eds.), *Toxic phytoplankton blooms in the sea* (pp. 245–249). Amsterdam: Elsevier.

Freeland, H. J. (1989). Observations of the low-frequency circulation off the west coast of British Columbia, Canada. In S. J. Neshyba, Ch. N. K. Moores, R. L. Smith, & R. T. Barber (Eds.), (pp. 132–139). *Poleward flows along ocean eastern boundaries, coastal and estuarine studies*, Vol. 34. Berlin: Spinger.

Frouin, R., Fiúza, A. F. G., Ambar, I., & Boyd, T. J. (1990). Observations of a poleward surface current off the coasts of Portugal and Spain during winter. *Journal of Geophysical Research, 95*, 679–691.

Gordon, H. R., & Wang, M. H. (1994). Retrieval of water-leaving radiance and aerosol optical-thickness over the oceans with seawifs - a preliminary algorithm. *Applied Optics, 33*, 443–452.

Hansen, H. P., & Grasshoff, K. (1983). Automated chemical analysis. In K. Grasshoff, M. Ehrhardt, & K. Kermling (Eds.), *Methods of seawater analysis* (2nd ed.) (pp. 347–395). Wheinheim: Verlag Chemie.

Haynes, R., & Barton, E. D. (1990). A poleward flow along the Atlantic coast of the Iberian Peninsula. *Journal of Geophysical Research, 95*, 11425–11441.

Haynes, R., & Barton, E. D. (1991). Lagrangian observations in the Iberian Coastal Transition Zone. *Journal of Geophysical Research, 96*, 14731–14741.

Haynes, R., Barton, E. D., & Pilling, I. (1993). Development, persistence and variability of upwelling filaments off the Atlantic Coast of the Iberian Peninsula. *Journal of Geophysical Research, 98*, 22681–22692.

Hidy, G. M. (1972). A view of recent air–sea interaction research. *Bulletin of the American Meteorological Society, 53*, 1083–1102.

Huthnance, J. M. (1995). Circulation, exchange and water masses at the ocean margin: the role of physical processes at the shelf edge. *Progress in Oceanography, 35*, 353–431.

Huyer, A., Kosro, P. M., Lentz, S. J., & Beardsley, R. C. (1989). Poleward flow in the California Current System. In S. J. Neshyba, Ch. N. K. Moores, R. L. Smith, & R. T. Barber (Eds.), (pp. 142–156). *Poleward flows along ocean eastern boundaries, coastal and estuarine studies*, Vol. 34. Berlin: Spinger.

Ibanez, F., Dauvin, J. C., & Ettienne, M. (1993). Comparison des evolutions à long-term (1977–1990) de deux peuplements macrobenthiques de la bahie de Morlaix (Manche Occidentale): relations avec les facteurs hycroclimatiques. *Journal of the Experimental Marine Biology and Ecology, 16*, 181–214.

Joint, I., Groom, S., Wollast, R., Chou, L., Tilstone, G. H., Figueiras, F. G., Loijens, M., & Smyth, T. J. (2002). The response of phytoplankton production to periodic upwelling and relaxation events at the Iberian shelf break: estimates by the ^{14}C method and by satellite remote sensing. *Journal of Marine Systems, 32*, 219–238.

Joint, I., Inall, M., Torres-Almarza, R., Figueiras, F. G., Álvarez-Salgado, X. A., & Woodward, M. (2001). Two Lagrangian experiments in the Iberian upwelling system: tracking an upwelling event and an off-shore filament. *Progress in Oceanography, 51*, 221–248.

Kiefer, D. A., Olson, R. J., & Holm-Hansen, O. (1976). Another look at the nitrite and chlorophyll maxima in the central North Pacific. *Deep-Sea Research, 23*, 1199–1208.

Krauss, W., & Käse, R. (1984). Mean circulation and eddy kinetic energy in the Eastern North Atlantic. *Journal of Geophysical Research, 89*, 3407–3415.

Lavender, S. J., & Groom, S. B. (1999). The seaWiFS automatic data processing system (SeaAPS). *International Journal of Remote Sensing, 20*, 1051–1056.

Lavín, A., Díaz del Río, G., Cabanas, J. M., & Casas, G. (1991). Afloramiento en el noroeste de la península Ibérica. Indices de afloramiento para el punto 43 grados N y 11 grados W periodo 1966–1989. *InformesTécnicos del Instituto Español de Oceanografía, 91*, 40.

Mazé, J. P., Arhan, M., & Mercier, H. (1997). Volume budget of the eastern boundary layer off the Iberian Peninsula. *Deep-Sea Research I, 44*, 1543–1574.

McClain, E. P., Pichel, W. G., & Walton, C. C. (1985). Comparative performance of AVHRR-based multichannel sea-surface temperatures. *Journal of Geophysical Research, 90*, 11587–11601.

McCreary, J. P., Shetye, S. R., & Kundu, P. J. (1986). Thermohaline forcing of eastern boundary currents with application to the circulation off the west coast of Australia. *Journal of Marine Research, 44*, 71–92.

McLain, C. R., Chao, S. -Y., Atkinson, L. P., Blanton, J. O., & de Castillejo, F. F. (1986). Wind-driven upwelling in the vicinity of Cape Finisterre. *Journal of Geophysical Research, 91*, 8470–8486.

Miller, P., Groom, S., McManus, A., Selley, J., & Mironnet, N. (1997). PANORAMA: a semi-automated AVHRR and CZCS system for observation of coastal and ocean processes. RSS97: observations and interactions. In *Proceedings of the remote sensing society* (pp. 539–544). Reading, September 1997.

Mooers, C. N. K. (1989). Workshop summary: poleward flow-observational and theoretical issues. In S. J. Neshyba, Ch. N. K.

Moores, R. L. Smith, & R. T. Barber (Eds.), (pp. 2–16). *Poleward flows along ocean eastern boundaries, coastal and estuarine studies*, Vol. 34. Berlin: Spinger.

Mouriño, C., & Fraga, F. (1985). Determinación de nitratos en agua de mar. *Investigación Pesquera*, *49*, 81–96.

Nelson, D. M., Treguer, P., Brzezinski, M., Leynaert, A., & Queguiner, B. (1995). Production and dissolution of biogenic silica in the ocean: revised global estimates, comparison with regional data and relationship to biogenic sedimentation. *Global Biogeochemical Cycles*, *8*, 359–372.

Nogueira, E., Pérez, F. F., & Ríos, A. F. (1997). Seasonal patterns and long-term trends in an estuarine upwelling ecosystem (Ría de Vigo, NW Spain). *Estuarine, Coastal and Shelf Science*, *44*, 285–300.

Olson, R. J. (1981a). Differential photoinhibiton of marine nitrifying bacteria: a possible mechanism for the formation of the primary nitrite maximum. *Journal of Marine Research*, *39*, 227–238.

Olson, R. J. (1981b). ^{15}N Tracer studies of the primary nitrite maximum. *Journal of Marine Research*, *39*, 203–225.

O'Reilly, J. E., Maritorena, S., Mitchell, B. G., Siegel, D. A., Carder, K. L., Garver, S. A., Kahru, M., & McClain, C. (1998). Ocean color chlorophyll algorithms for SeaWiFS. *Journal of Geophysical Research*, *103*, 24937–24953.

Pelíz, A. J., & Fiúza, A. F. G. (1999). Temporal and spatial variability of CZCS-derived phytoplankton pigment concentration off the western Iberian Peninsula. *International Journal of Remote Sensing*, *20*, 1363–1403.

Pérez, F. F., Álvarez-Salgado, X. A., Rosón, G., & Ríos, A. F. (1992). Carbonic-calcium system, nutrients and total organic nitrogen in continental runoff to the Galician Rías Baixas, NW Spain. *Oceanologica Acta*, *15*, 595–602.

Pérez, F. F., Castro, C. G., Álvarez-Salgado, X. A., & Ríos, A. F. (2001a). Coupling between the Iberian margin scale circulation and the eastern boundary Portugal current. *Deep-Sea Research I*, *48*, 1519–1533.

Pérez, F. F., Castro, C. G., Álvarez-Salgado, X. A., & Ríos, A. F. (2001b). Coupling between the Iberian basin-scale circulation and the Portugal boundary current system. A chemical study. *Deep-Sea Research I*, *48*, 1519–1533.

Pérez, F. F., & Fraga, F. (1987a). The pH measurements in seawater on NBS scale. *Marine Chemistry*, *21*, 315–327.

Pérez, F. F., & Fraga, F. (1987b). A precise and rapid analytical procedure for alkalinity determination. *Marine Chemistry*, *21*, 169–182.

Pérez, F. F., Mouriño, C., Fraga, F., & Ríos, A. F. (1993). Displacement of water masses and remineralization rates off the Iberian Peninsula by nutrient anomalies. *Journal of Marine Research*, *51*, 869–892.

Pérez, F. F., Ríos, A. F., King, B. A., & Pollard, R. T. (1995). Decadal changes of θ–S relationship of the Eastern North Atlantic Central Water (ENAW). *Deep-Sea Research I*, *42*, 1849–1864.

Pérez, F. F., Ríos, A. F., & Rosón, G. (1998). Sea surface carbon dioxide off the Iberian Peninsula (North Eastern Atlantic Ocean). *Journal of Marine Systems*, *19*, 27–46.

Pilskaln, C. H., Paduan, J. B., Chavez, F. P., Anderson, R. Y., & Berelson, W. M. (1996). Carbon export and regeneration in the coastal upwelling system of Monterey Bay, central California. *Journal of Marine Research*, *54*, 1149–1178.

Pingree, R. D. (1994). Winter warming in the southern Bay of Biscay and Lagrangian eddy kinematics from a deep-drogued argos buoy. *Journal of the Marine Biological Association of the UK*, *74*, 107–128.

Pingree, R. D., & Le Cann, B. (1989). Celtic and Armorican slope and shelf residual currents. *Progress in Oceanography*, *23*, 303–338.

Pingree, R. D., & Le Cann, B. (1990). Structure, strength and seasonality of the slope currents in the Bay of Biscay region. *Journal of the Marine Biological Association of the UK*, *70*, 857–885.

Pingree, R. D., Sinha, B., & Griffiths, C. R. (1999). Seasonality of the European slope current (Goban Spur) and ocean margin exchange. *Continental Shelf Research*, *19*, 929–975.

Planet, W. G. (1988). Data extraction and calibration of TIROS-N/NOAA radiometers. *NOAA Technical Memorandum NESS 107 Rev 1, Washington*.

Platt, T., Gallegos, C. L., & Harrison, W. G. (1980). Photoinhibition of photosynthesis in natural assemblages of marine phytoplankton. *Journal of Marine Research*, *38*, 687–701.

Poularikas, A. D., & Seely, S. (1991). In *Signals and systems* (2nd ed.) (p. 1015). Boston: PWS-KENT Publishing Company.

Prego, R., & Bao, R. (1997). Upwelling influence on the Galician coast: silicate in shelf waters and underlying surface sediments. *Continental Shelf Research*, *17*, 307–318.

Rault, P. L., Sohier, L. P., Rivier, A. M., & Daumas, R. A. (1988). Dark bacterial-protozoan culture: acidification, nitrite accumulation and protozoan inhibition in the absence of phytoplankton. *Journal of the Experimental Biology and Ecology*, *116*, 273–291.

Reid, J. L., & Mantyla, A. W. (1976). The effect of the geostrophic flow upon coastal elevations in the northern North Pacific. *Journal of Geophysical Research*, *81*, 3100–3110.

Richardson, P. L. (1983). Eddy kinetic energy in the North Atlantic from surface drifters. *Journal of Geophysical Research*, *88*, 4355–4367.

Ríos, A. F., Pérez, F. F., & Fraga, F. (1992). Water masses in upper and middle North Atlantic Ocean east of the Azores. *Deep-Sea Research I*, *39*, 645–658.

Smith, R. L. (1989). Poleward flows along eastern ocean boundaries: an introduction and historical review. In S. J. Neshyba, Ch. N. K. Moores, R. L. Smith, & R. T. Barber (Eds.), (pp. 17–24). *Poleward flows along ocean eastern boundaries, coastal and estuarine studies*, Vol. 34. Berlin: Spinger.

Smith, R., Huyer, A., Godfrey, S., & Church, J. (1991). The Leeuwin current off Western Australia, 1986–1987. *Journal of Physical Oceanography*, *21*, 323–345.

Swallow, J. C., Gould, W. J., & Saunders, P. M. (1977). Evidence for a poleward eastern boundary current in the North Atlantic Ocean. *ICES hydrography committee*, C.M. 1977/c:32 (21 pp).

Takahashi, M., Nakai, T., Ishimaru, T., Hasumoto, H., & Fujita, Y. (1985). Distribution of the subsurface chlorophyll maximum and its nutrient-light environment in and around the Kuroshio off Japan. *Journal of the Oceanographical Society of Japan*, *41*, 73–80.

Teira, E., Serret, P., & Fernández, E. (2001). Phytoplankton size-structure, particulate and dissolved organic carbon production and oxygen fluxes through microbial communities in the NW Iberian coastal transition zone. *Marine Ecology Progress Series*, *219*, 65–83.

UNESCO (1986). Progress on oceanographic tables and standards 1983-1986. Work and recommendations of UNESCO/SCOR/ICES/IAPSO Joint panel. UNESCO Technical Papers in Marine Science 50.

Vaccaro, R. F., & Ryther, J. H. (1960). Marine phytoplankton and the distribution of nitrite in the sea. *Journal du Conseil Permanent International pour l'Exploration de la Mer*, *25*, 260–271.

Vázquez, J., Hamilton, M., Van Tran, A., & Sumagaysay, R. M. (1994). JPL physical oceanography DAAC reprocesses ten years of sea-surface temperature measurements from NOAA AVHRR. *The Earth Observer*, *6*, 16–17.

Wada, E., & Hattori, A. (1991). *Nitrogen in the Sea: forms, abundances, and rate processes*. Boca Raton: CRC Press.

Wooster, W. S., Bakun, A., & Mclain, D. R. (1976). The seasonal upwelling cycle along the eastern boundary of the North Atlantic. *Journal of Marine Research*, *34*, 131–141.

Yentsch, C. S., & Menzel, D. W. (1963). A method for the determination of phytoplankton chlorophyll and phaeophytin by fluorescence. *Deep-Sea Research*, *10*, 221–231.